New Random Copolymer Acceptors Enable Additive-Free Processing of 10.1% Efficient All-Polymer Solar Cells with Near Unity Internal Quantum Efficiency

Nagesh B. Kolhe, [†‡] Duyen K. Tran, [†‡] Hyunjong Lee, [†‡] Daiki Kuzuhara, [§] Noriyuki Yoshimoto,[§] Tomoyuki Koganezawa,[‖] and Samson A. Jenekhe*,[†]

[†]Department of Chemical Engineering and Department of Chemistry, University of Washington, Seattle, Washington 98195-1750, USA

[§]Faculty of Science and Engineering, Iwate University, 4-3-5 Ueda, Morioka, Iwate, 020-8551, Japan

[‖]Industrial Application Division, Japan Synchrotron Radiation Research Institute, Sayo, Hyogo, 679-5198, Japan

ABSTRACT: Finding effective molecular design strategies to optimize the active layer blend morphology is among the longstanding challenges in developing efficient all-polymer solar cells (all-PSCs). Here we show that new biselenophene/selenophene-linked naphthalene diimide random copolymer acceptors BSS*x* (*x* = 10, 20, 50) facilitate the achievement of high performance all-PSCs without the use of any solution processing additive. Blends of BSS10 with donor polymer PBDB-T combined 10.1% power conversion efficiency with 97% internal quantum efficiency and 0.59 eV optical bandgap energy loss (E_{loss}). BSS10- and BSS20-based devices have the best combination of high external quantum efficiency (>85%) and small E_{loss} (<0.6 eV) among all-PSCs yet reported. The results demonstrate that the blend morphology, charge carrier mobilities, and photovoltaic properties of all-PSCs could be rationally optimized by means of a synthetic variable – the random copolymer composition.

TOC GRAPHICS

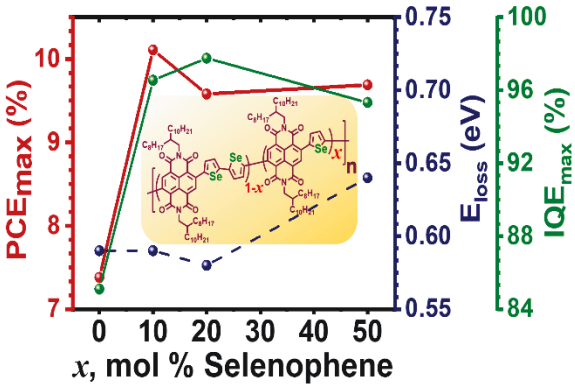

Emergence and rapid advances in non-fullerene acceptors (NFAs) in the last 5 years have opened up new pathways to improve the performance of polymer solar cells.[1-5] In the case of small-molecule NFAs based single-junction and tandem cells, power conversion efficiencies (PCEs) exceeding 15% and 17%, respectively, have been reported.[6, 7] Although there has been similar recent progress in developing all-polymer solar cells (all-PSCs),[8-11] binary blends of an electron-accepting polymer and a donor polymer, state-of-the-art single junction devices have PCEs of 8-10% and thus significantly lag behind small-molecules NFAs based polymer solar cells.[12-23] A major challenge in further improvement of the performance of all-PSCs is how to simultaneously increase the short-circuit current (J_{sc}) and fill factor (FF), which are both critically dependent on the blend morphology.[8, 24-28]

Various approaches to the control and optimization of the active layer blend morphology of all-PSCs have been explored to varying degrees of success in improving the device performance, including: solution processing additives;[18-21, 29-31] side chain engineering of the acceptor polymer component;[32-34] co-solvents;[35] post-deposition treatment such as solvent vapor annealing[36] and room temperature annealing termed "aging".[12, 18] We have previously reported that perylene diimide (PDI)/naphthalene diimide (NDI) random copolymers can function as the acceptor component in all-PSCs and facilitate control of the bulk crystallinity, blend morphology, and device performance.[24] Indeed, other groups have similarly found that random copolymer or terpolymer acceptors can lead to improved performance of all-PSCs.[20, 37-40] However, even in these cases of random copolymer acceptor based all-PSCs, the use of a solution processing additive was necessary to achieve optimal blend morphology and highly efficient devices.[20, 21]

In this paper, we show that highly efficient (>10%) single-junction all-PSCs can be developed from new NDI-biselenophene/NDI-selenophene random copolymer acceptors BSS*x* (*x*

= 10, 20, 50) without the use of any solution processing additive. The active layer blend morphology, charge carrier mobilities, and photovoltaic properties of the all-PSCs were found to vary substantially with the random copolymer composition. We found that blends of the optimum random copolymer composition, BSS10, with donor PBDB-T produced all-PSCs with 10.1% PCE, a high IQE of 97%, and a low E_{loss} of 0.59 eV. The photovoltaic properties (J_{sc}, V_{oc}, FF, PCE) of all-PSCs based on the random copolymer acceptors were substantially enhanced compared to the reference BSS0 devices. These results show that random copolymer architectures represent a promising general strategy towards further advances in all-PSCs.

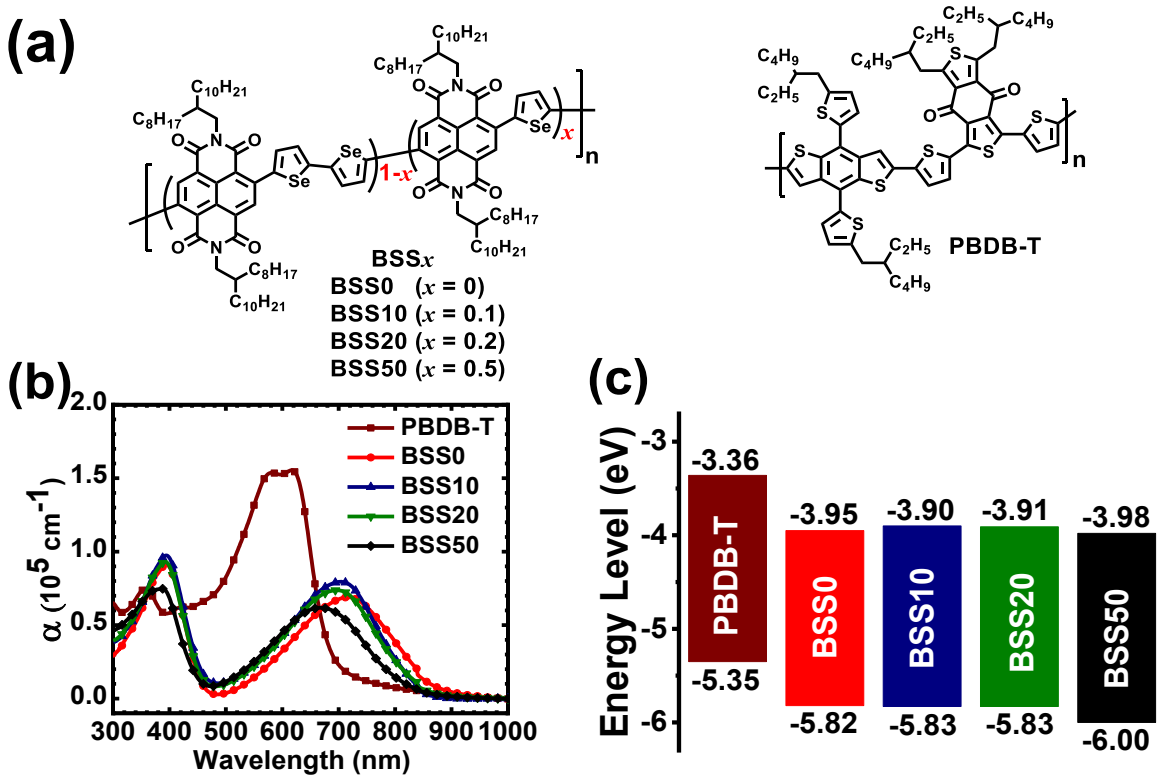

Figure 1. (a) Molecular structures of random copolymer acceptors (BSS*x*) and donor polymer (PBDB-T). (b) Thin film optical absorption spectra of PBDB-T and BSS*x* (*x* = 0, 10, 20, 50). (c) HOMO/LUMO energy levels of donor polymer and random copolymer acceptors.

The new random copolymers, BSS*x* (*x* = 0, 10, 20, 50) in which the biselenophene and selenophene linkages are statistically distributed in the chain (Figure 1), were synthesized by Stille coupling polymerization of 4,9-dibromo-2,7-bis(2-octyldodecyl)-benzo[lmn] [3,8]-phenanthroline-1,3,6,8-tetraone with 5,5'-bis(trimethylstannyl)-2,2'selenophene and 2,5-bis(trimethylstannyl)-selenophene following the general literature procedures.[24, 41, 42] The BSS*x* samples showed excellent solubility in organic solvents (e.g. chloroform, chlorobenzene, and dichlorobenzene). Their molecular structures were confirmed by ^{1}H NMR spectra (Figure S1) and molecular weight obtained by gel permeation chromatography (GPC) in 1,2,3-trichlorobenzene solvent at 120 °C had a number-average molecular weight (M_n) in the range of 28.4-41.7 kDa with a dispersity ($Đ$) of 2.02-2.88 (Table S1). The copolymers had an onset decomposition temperature (T_d) > 385 °C (Table S1 and Figure S2) and differential scanning colorimetry (DSC) scans (Figure S3) showed that the BSS*x* (*x* = 10, 20, 50) copolymers had lower melting transition (T_m) and melting enthalpy (ΔH_m) (Table S1) than the reference BSS0 homopolymer. The DSC results indicate that the random copolymers have reduced crystallinity and different molecular ordering compared to the reference BSS0.

The thin film optical absorption spectra of BSS*x* copolymers and donor polymer PBDB-T are shown in Figure 1b. The absorption spectra of BSS*x* show the characteristic two-bands similar to the known BSS0 spectrum.[18, 41] The main changes with copolymer composition occur in the intramolecular charge transfer (ICT) band (500-850 nm). The absorption maximum (λ_{max}) of the ICT band at 720 nm in BSS0 is progressively blue shifted to 703 nm in BSS10, 698 nm in BSS20, and 668 nm in BSS50 (Table S1). The optical bandgap (E_g^{opt}) increases slightly from 1.40 eV for BSS0 to 1.44 eV for both BSS10 and BSS20 and 1.49 eV for BSS50. The HOMO/LUMO energy levels of the random copolymers were measured by using the onset redox potentials from cyclic

voltammetry (CV) and are shown in Figure 1c. The energy levels vary only slightly with copolymer composition except in BSS50 where the HOMO level was downshifted to -6.0 eV, because its CV scan did not show an oxidation peak up to 2V which implies the HOMO energy level was either at or lower lying than -6.0 eV.[12] The electronic energy level offsets at the BSS*x*/PBDB-T interfaces are ideal for efficient photoinduced charge transfer.[43]

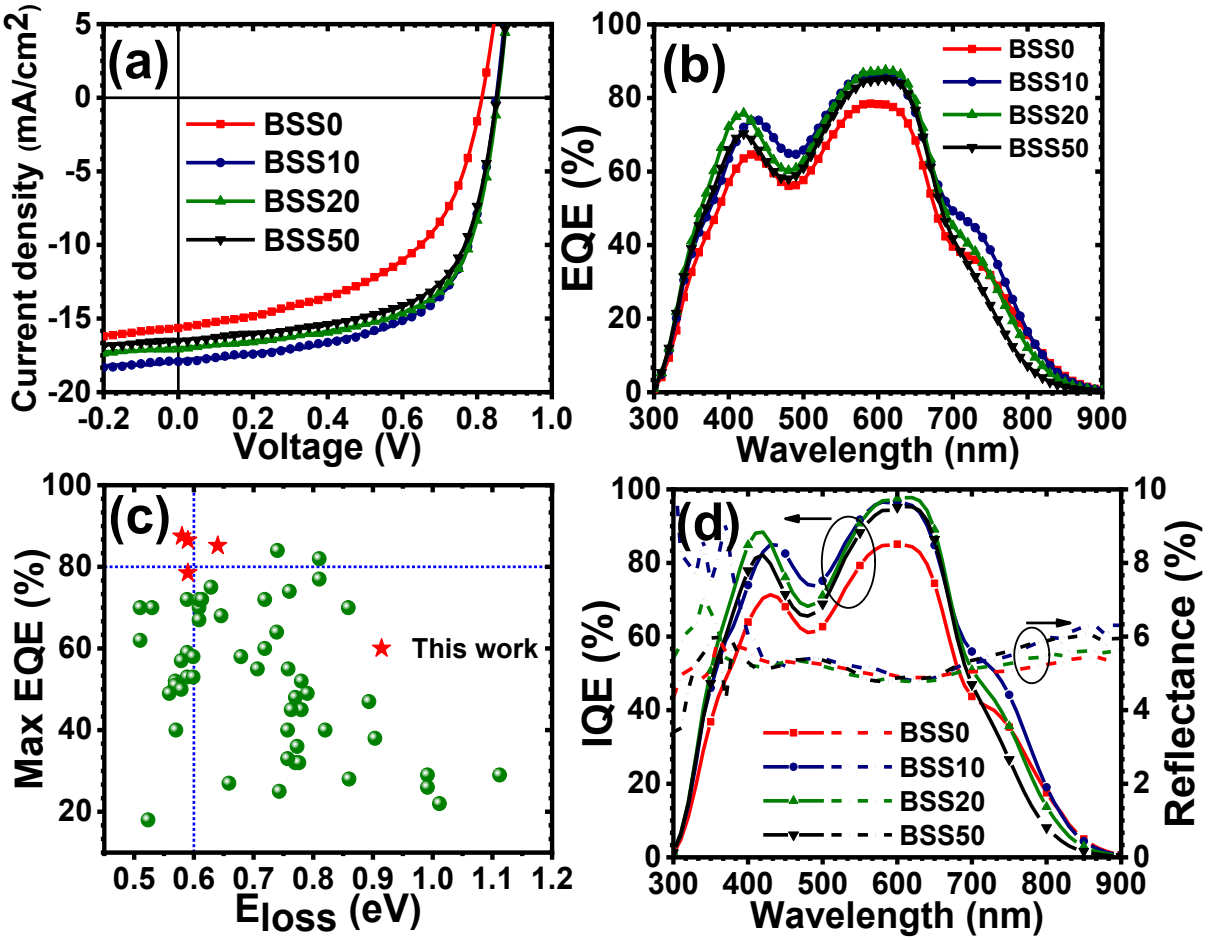

Figure 2. (a) Current density (J_{sc})-Voltage (V) characteristics. (b) EQE spectra for the optimal BSS*x*:PBDB-T all-polymer solar cells. (c) Maximum EQE versus the optical bandgap energy loss ($E_{loss} = E_g - qV_{oc}$) for published all-PSCs[12, 14, 17, 18, 24, 32, 37, 44-52] and the present work. (d) IQE spectra for the optimal BSS*x*:PBDB-T all-polymer solar cells. All the blend active layers were thermally annealed at 175 °C for 10 min without the use of any processing additives.

The photovoltaic properties of all-PSC devices incorporating each of the new random copolymers (BSS*x*) as the electron acceptor component and PBDB-T as the donor polymer were

investigated by fabricating and evaluating all-PSC devices with inverted structure: ITO/ZnO/PEI/blend/MoO_3/Ag, where polyethyleneimine (PEI) is a cathode interface layer.[53] Each BSS*x*:PBDB-T blend active layer was prepared under optimized conditions of blend ratio 0.6:1 (wt:wt), spin coating from chlorobenzene solution, and thermal annealing at 175 °C for 10 min *without* using any solvent additives or special post-processing treatment. The reference BSS0:PBDB-T blend devices were fabricated and evaluated under identical conditions to facilitate consistent comparison. The current density-voltage (*J-V*) curves and the external quantum efficiency (EQE) spectra of all-PSC devices are given in Figure 2a and 2b, respectively. The associated photovoltaic parameters, including the short-circuit current density (J_{sc}), the open-circuit voltage (V_{oc}), fill factor (FF), and PCE, are summarized in Table 1.

Table 1. Photovoltaic Properties of Thermally Annealed (175 °C for 10 min) BSS*x*:PBDB-T (0.6:1 wt/wt) All-Polymer Solar Cells.

Blend	J_{sc} [(a)] (mA/cm^2)	V_{oc} [(a)] (V)	FF[(a)]	PCE [(a)] (%)	Calc. J_{sc} (mA/cm^2)	EQE_{max} (%)	IQE_{max} (%)
BSS0	15.74 (15.64 ± 0. 35)	0.82 (0.81 ± 0.004)	0.57 (0.53 ± 0. 02)	7.38 (6.71 ± 0. 31)	15.43	78.5	85.1
BSS10	18.55 (17.92 ± 0. 26)	0.86 (0.85 ± 0.003)	0.64 (0.63 ± 0. 01)	10.1 (9.59 ± 0. 16)	17.51	86.5	96.6
BSS20	17.07 (17.07 ± 0. 28)	0.86 (0.86 ± 0.004)	0.65 (0.64 ± 0. 01)	9.58 (9.35 ± 0. 18)	16.98	87.5	97.8
BSS50	17.50 (16.53 ± 0. 35)	0.86 (0.85 ± 0.004)	0.65 (0.64 ± 0. 01)	9.69 (8.97 ± 0. 36)	16.89	85.2	95.3

(a) Average values provided in the parentheses with standard deviation were obtained from 16 devices.

The reference BSS0:PBDB-T devices have a maximum PCE of 7.4% with J_{sc} of 15.64 mA/cm^2, V_{oc} of 0.81 V, and FF of 0.53 (Figure S13). This performance is in good agreement with our previously reported all-PSCs with a similar blend active layer processed under thermal annealing condition.[18] Compared to the reference BSS0:PBDB-T blend, all-PSC devices based on the random copolymer acceptors, BSS10:PBDB-T and BSS20:PBDB-T, were found to exhibit

significantly enhanced photovoltaic performance. Notably, the fill factor increased from 0.53 in BSS0 devices to 0.63 in BSS10 devices and to 0.64 in BSS20 and BSS50 devices. The V_{oc} also increased slightly from 0.81V to 0.85 – 0.86V in the BSS10, BSS20, and BSS50 devices (Table 1). The J_{sc} increased to a maximum of 17.92 mA/cm^2 in the BSS10 all-PSCs and then decreased progressively to 16.53 mA/cm^2 in the BSS50 devices. As a result of these copolymer composition dependent changes in FF, V_{oc}, J_{sc}, the best PCE of 10.1% was obtained in the BSS10 devices and this was followed by 9.6% - 9.7% achieved in BSS20- and BSS50- containing all-PSCs (Figure S13). Examination of the average PCE dependence on the copolymer composition shows that it increased significantly from 6.7% in BSS0 to a peak of 9.6% in BSS10 and then decreased to 9.0% in BSS50 (Table 1). We conclude that BSS10 and BSS20 compositions of the random copolymer acceptor BSS*x*, are close to the optimum value. Furthermore, these results demonstrate that the photovoltaic properties of the random copolymer acceptors BSS10, BSS20, and BSS50 are all substantially enhanced compared to the reference BSS0 (or PNDIBS) and thus that each random copolymer acceptor blend with the donor polymer PBDB-T is more compatible than BSS0:PBDB-T blends.

The use of solvent additives and different post-processing treatments as a means of optimizing the photovoltaic blend morphology and thus to enhance the efficiency of polymer solar cells is well established in the OPV field,[29, 54] including all-PSCs.[19] Indeed, we have previously found that use of a processing additive in the fabrication of all-PSCs from the reference polymer, PNDIBS (or BSS0), led to significantly enhanced performance.[18] We have thus explored various processing additives, including diphenyl ether (DPE), 1,8-octanedithiol (ODT), 1-chloronapthalene (CN), and 1,8-diiodooctane (DIO), in the fabrication of all-PSCs from the present random copolymer acceptors, BSS*x*. Representative *J*-*V* curves of such all-PSCs are given

in Figures S6 and S7 while the associated photovoltaic parameters are summarized in Tables S2 and S3. We found that for the random copolymer acceptor based all-PSCs, however, the use of any of the series of processing additives resulted in a significant reduction in performance relative to the simple thermally annealed (175^{o}C, 10 min) devices. These results are in stark contrast to prior reports on all-PSCs based on either homopolymer acceptors[18] or random copolymer acceptors,[20, 24, 36, 37] where optimal active layer morphology and best device performance were achieved by using processing additives. Our present results demonstrate that a solvent additive is not necessary for achieving optimal high performance in all-PSCs based on the new random copolymer acceptors, BSS*x*, and imply that optimal active layer morphology is obtained by a simple thermal annealing.

The EQE spectra of the best BSS*x*:PBDB-T all-PSCs are shown in Figure 2b. In the cases of the reference BSS0 (PNDIBS) and the random copolymer BSS10 and BSS20 blend devices, photocurrent generation starting from 885 nm and extending to 300 nm is observed and nicely matches the complementary absorption spectra of the component donor (PBDB-T) and acceptor polymers (Figure 1b). However, the BSS50:PBDB-T blend device has a photocurrent response that starts from 830 nm and extends to 300 nm in accord with the absorption spectrum (Figure 1b). It is clear that photocurrent generation in the 450 – 650 nm region originates primarily from photoinduced electron transfer from the donor polymer, PBDB-T, while photocurrent generation in the 350 – 450 nm and 680 – 880 nm regions comes from efficient photoinduced hole transfer from the acceptor polymer, BSS*x*. The maximum EQE values were found in the 560 – 660 nm range: ~ 87 – 88% for BSS10 and BSS20 devices; ~ 85% for BSS50 devices; and ~ 79% for the reference BSS0 all-PSCs. Although the EQE spectrum of the reference BSS0 covers the same light harvesting wavelength range as those of the random copolymer acceptors, the latter clearly have

the superior quantum efficiency in agreement with the previously discussed enhanced J_{sc} values. The photocurrent J_{sc} values obtained by integrating the EQE spectra were found to be within 1 – 4% mismatch with the values obtained from *J-V* measurements (Table 1).

Prior observations[12, 17, 55] of high EQE values (> 80%) in all-PSCs were found to be accompanied by large optical bandgap energy loss ($E_{loss} = E_g^{opt} - qV_{oc}$) while those with small E_{loss} values (< 0.6 eV) generally had low EQE (< 70%) as illustrated in Figure 2c. The E_{loss} values of the present all-PSCs were 0.59 eV, 0.59 eV, 0.58 eV, and 0.64 eV, respectively for BSS0, BSS10, BSS20, and BSS50 devices. Although the BSS50:PBDB-T devices exhibit an impressive EQE (> 85%), the large E_{loss} value compared to the reference BSS0 devices is a consequence of the larger optical bandgap of BSS50 (Table S1). As displayed in the EQE versus E_{loss} plot of Figure 2c, we find that the present BSS10- and BSS20-based all-PSCs show the best combination of high EQE (> 85%) and small E_{loss} (< 0.6 eV) among reported all-PSCs to date. Although the detailed mechanism underlying the combination of high EQE with small E_{loss} among these or any all-PSCs remains to be fully understood,[56, 57] it is clear that the random copolymer architecture of the present acceptor copolymers (BSS10 and BSS20) plays a key role. We propose that since the HOMO/LUMO energy levels that largely determine the V_{oc} as well as the optical band gap (E_g^{opt}) are not significantly modified by random copolymerization, E_{loss} will remain small and comparable to the reference homopolymer BSS0. On the other hand, the random copolymer acceptors facilitate an optimal blend morphology, which in turn enables enhanced photocurrent generation or higher EQE compared to the BSS0 devices.

To fully understand the observed high EQE values of the BSS*x* random copolymers based all-PSCs, we measured the internal quantum efficiency (IQE) which is the ratio of the number of

charge carriers extracted to the number of photons absorbed in the photoactive layer. The IQE spectrum was collected by normalizing the EQE spectrum to the light absorption spectrum measured in reflectance with an integrating sphere.[58] The IQE spectra (Figure 2d) of BSS*x*:PBDB-T all-PSCs show IQE values exceeding 80% in the 520 – 660 nm region with peak values of 85.1% at 600 nm in BSS0 devices and 95 – 98% at around 600 – 620 nm in the random copolymer acceptor (BSS10, BSS20, and BSS50) devices (Table 1). IQE values approaching 100% in BSS10 and BSS20 devices suggest that nearly all absorbed photons in these random copolymer blends create excitons that are effectively dissociated and collected as charges at electrodes. The near unity IQE obtained in BSS10 and BSS20 devices also strongly suggests that an ideal blend morphology is achieved with optimal phase separation for efficient charge generation, charge transport, and charge collection.[59]

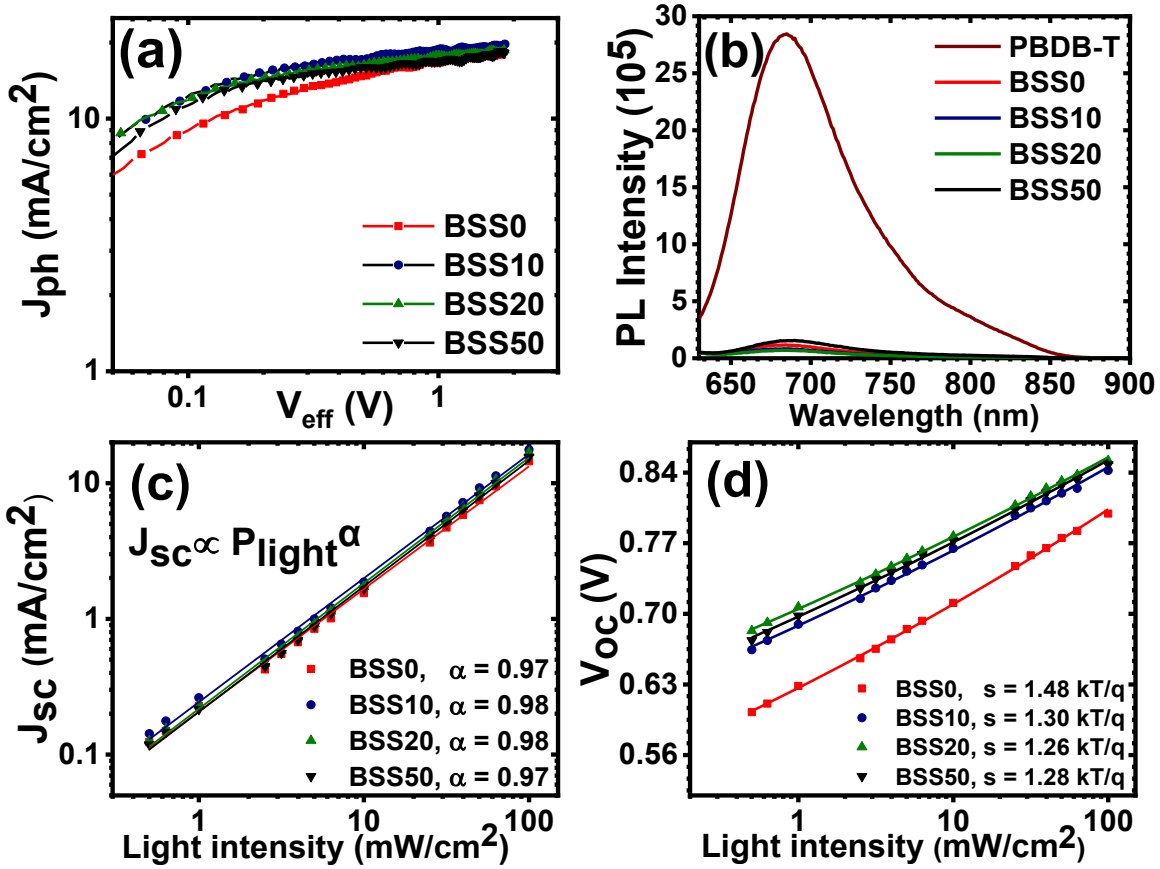

Figure 3. (a) J_{ph}-V_{eff} curves of BSS*x*:PBDB-T blend films. (b) PL emission spectra (600-nm excitation) of neat PBDB-T donor film and BSS*x*:PBDB-T blend films. (c) J_{sc} dependence on light intensity for BSS*x*:PBDB-T blend (0.6:1 wt:wt) all-PSCs. (d) V_{oc} dependence on light intensity for BSS*x*:PBDB-T blend (0.6:1 wt:wt) all-PSCs.

We evaluated the photoinduced charge carrier generation and charge collection behavior in the BSS*x*:PBDB-T blend devices by analyzing the photocurrent density J_{ph} ($J_{ph} = J_L - J_D$) versus effective voltage V_{eff} ($V_{eff} = V_{bi} - V_a$) curves (Figure 3a), where J_L and J_D are the current densities under illumination and dark conditions, respectively, and V_{bi} is the built-in-voltage or the voltage when $J_{ph} = 0$ and V_a is the applied voltage. For all the devices, J_{ph} saturates at high V_{eff} values of about 2V, resulting in a saturation photocurrent density (J_{sat}) of 19.7 mA/cm^2 in BSS10, 18.6 mA/cm^2 in BSS20, 18.2 mA/cm^2 in BSS50, and 17.9 mA/cm^2 in BSS0. We conclude that the effective voltage is large enough to extract nearly all photogenerated free charges to the electrode at the saturation point.[60] Therefore, maximum photoinduced carrier generation rate G_{max} can be estimated from the J_{sat}: ($G_{max} = J_{sat}/ q.L$), where q is the elementary charge and L is active layer thickness. Among the all-PSCs, devices based on copolymer BSS10 and BSS20 showed the highest G_{max} value of 1.23 x10^{26} m^{-3} s^{-1} and 1.16 x10^{26} m^{-3} s^{-1}, respectively, while the BSS50 and BSS0 devices yielded lower G_{max} values of 1.13 x10^{26} m^{-3} s^{-1} and 1.11 x10^{26} m^{-3} s^{-1}, respectively. The higher G_{max} values imply that more efficient light absorption and exciton dissociation occur in the BSS10- and BSS20-based devices as compared to the other all-PSCs. This is likely due to the optimal morphology in the BSS10 and BSS20 blends and further give support to the observed increased J_{sc} in BSS10 and BSS20 devices compared to BSS50 and BSS0 devices.

We next investigated the charge collection capacity of the BSS*x*:PBDB-T blend devices by calculating the charge collection probability *P(E,T)* under short circuit condition. Higher values of

P (*E*, *T*), 94.1 % and 92.5 %, were found for BSS10 and BSS20 devices, respectively, as compared to 89.3% in BSS0 and 91.4 % in BSS50. These results suggest that the charge collection process is more efficient in the BSS10- and BSS20-based devices in agreement with the previously discussed photovoltaic properties.

We carried out photoluminescence (PL) quenching experiments to further understand the exciton dissociation and photoinduced charge transfer in the BSS*x*:PBDB-T solar cells. The PL emission spectra of neat PBDB-T thin film and its blends with the BSS*x* copolymers are shown in Figure 3b. PBDB-T exhibits a broad PL emission spectrum with a peak at 690 nm. The PL emission of PBDB-T blends was quenched 97% in BSS20, 96% in BSS10, 94% in BSS50, and 95% in BSS0. The strong quenching of the blend PL spectra suggests that the photoinduced charge transfer is highly efficient in all the devices. However, the slightly higher PL emission quenching efficiency in BSS10 and BSS20 blends as compared to BSS50 and BSS0 indicates that the BSS10 and BSS20 blend devices have a blend morphology with small phase-separated domains that enabled efficient exciton dissociation.

To gain insights into the charge recombination kinetics of the random copolymers based all-PSC devices, we measured their current density (J_{sc}) as a function of illumination intensity (P_{light}). As shown in Figure 3c, J_{sc} follows the expected power-law dependence on P_{light} ($J_{sc} \propto P_{light}^{\alpha}$), where linearity ($\alpha = 1$) indicates all charge carriers are extracted prior to recombination.[61] The fitted lines in the J_{sc} versus P_{light} data resulted in comparable α values ($\alpha \sim 0.97 - 0.98$) for all four blends systems, which indicates that there is negligible bimolecular recombination in these systems. On the other hand, the light intensity dependence of V_{oc} shown in Figure 3d provide information regarding the competition between bimolecular and trap-assisted recombination in the

charge recombination dynamics of these all-PSCs. As seen in Figure 3d, BSS0 exhibits a steep slope of 1.48kT/q, which suggests that there is a mix of trap-assisted and bimolecular recombinations. In contrast, the BSS*x* (*x* = 10, 20, 50) devices show a smaller dependence of V_{oc} on light intensity with a slope of around 1.3kT/q. The stronger dependence of V_{oc} on P_{light} in the BSS0 devices corroborates with the observed trend in FF (Table 1); in particular, the BSS*x* (*x* = 10, 20, 50) blends show suppressed charge recombination, leading to an enhanced fill factor compared to the reference BSS0 devices.

We investigated the bulk charge carrier mobilities of the neat BSS*x* films and the BSS*x*:PBDB-T all-PSC blend films prepared under similar conditions as used for the solar cell devices by using the space charge limited current (SCLC) technique. The *J-V* curves and SCLC fittings of the data for blend devices are given in Figure S8 and in Figure S9 for neat films. The SCLC carrier mobilities are summarized in Table S4. The SCLC electron mobility (μ_e) of the BSS0 neat film was 3.49 x 10^{-5} cm^2/Vs. In contrast, the electron mobility was significantly enhanced in the random copolymer films, μ_e increased about 5-fold in BSS10 films (μ_e = 1.60 x 10^{-4} cm^2/Vs) and 7-fold in BSS20 films (μ_e = 2.42 x 10^{-4} cm^2/Vs). In BSS50 films the electron mobility slightly increased by a factor of 1.5 to μ_e = 5.35 x 10^{-5} cm^2/Vs. The observed large increase of the electron mobility in the neat random copolymer thin films compared to the reference BSS0 neat films suggest that the random copolymers have favorable *face-on* oriented molecular packing which will be discussed later with GIWAXS data. In the case of blend devices, the bulk electron mobility decreased relative to the neat films. However, similar to the observed trends in the neat films, the bulk electron mobility is significantly enhanced in the random copolymer blends compared to BSS0 blends. Electron mobility of 1.69 x 10^{-5} cm^2/Vs is seen in BSS0 blends but is enhanced 3.6 – 4 times in BSS10 and BSS20 blends and 1.3 times in BSS50

blends. The hole mobility is found to be enhanced by 2.8-fold in BSS10 blends (5.33 x 10^{-4} cm^2/Vs) and 2.3-fold in BSS20 blends (4.43 x 10^{-4} cm^2/Vs) as compared to BSS0 blends (1.89 x 10^{-4} cm^2/Vs) (Table S4). The hole mobility is decreased to 6.28 x 10^{-5} cm^2/Vs in the case of BSS50 blends. The observed substantial increase of carrier mobilities in the random copolymer thin films clearly suggests that the BSS*x*:PBDB-T blends have a more favorable bulk morphology for efficient charge transport than the reference BBS0:PBDB-T blends. Further examination of the bulk charge transport in these all-PSCs shows that the reference BSS0 blend devices have the most unbalanced carrier mobilities (μ_h/μ_e = 11.2) whereas μ_h/μ_e of 7.9 in BSS10, 7.2 in BSS20, and 2.9 in BSS50 were observed. We note that balanced charge transport (μ_h/μ_e ~ 1) and high charge carrier mobilities are highly desirable to reduce bimolecular recombination in solar cell devices and thereby maximize the photocurrent and FF value.[36, 62] However, we note that the μ_h/μ_e ratio is still too high in the random copolymer blend devices, which is a reason for the still low FF (0.64).

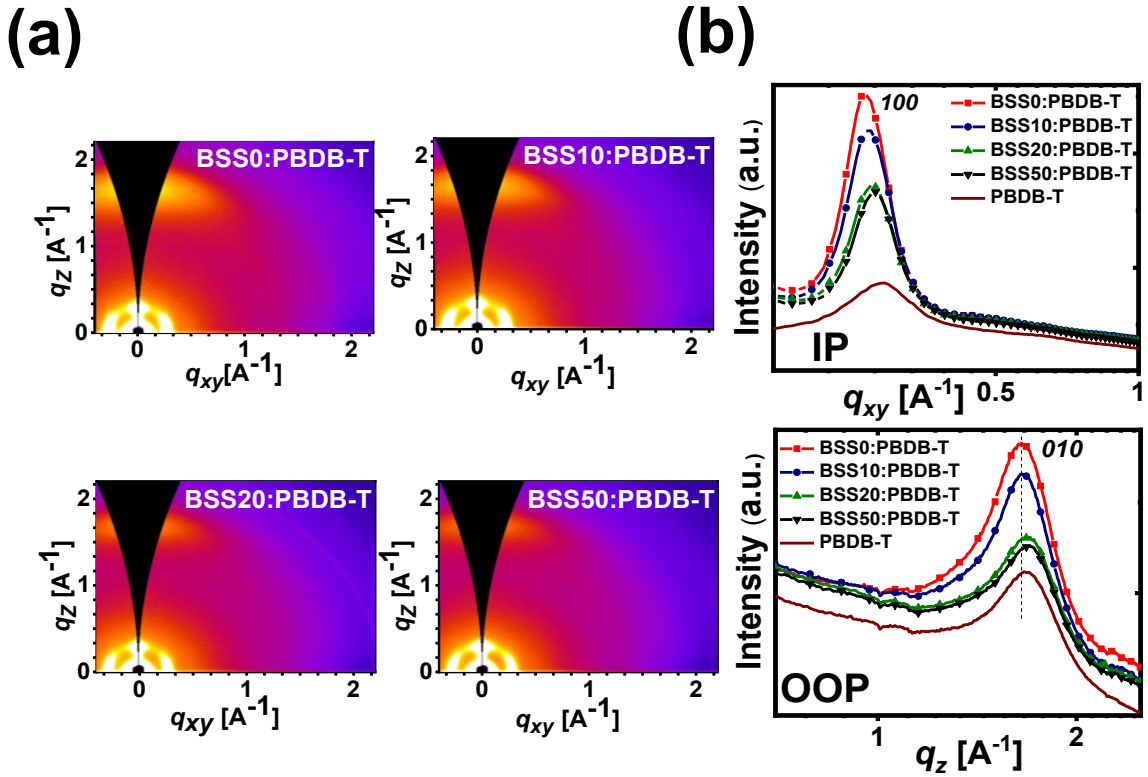

Figure 4. (a) 2D-GIWAXS images of BSS*x*:PBDB-T blend films, and (b) line cuts of GIWAXS patterns for in-plane (IP) and out-of-plane (OOP) directions.

The surface morphology of the BSS*x*:PBDB-T blend devices as well as the neat films of the component polymers was characterized by tapping-mode atomic force microscopy (AFM). AFM height and phase images of neat films of the component polymers and their blends are shown in Figures S10 and S11, respectively. All the neat films of BSS*x* showed similar granular morphology (Figure S10). Although BSS0 and BSS50 blend films showed indistinguishable morphology compared to their neat films, BSS10 and BSS20 blend films exhibited fibrillar morphology with smaller domain sizes (~ 10 – 15 nm) (Figure S11), thus suppressed macroscopic phase separation.

The thin film morphology of neat BSS*x* random copolymers and their blends with donor PBDB-T was characterized by 2D grazing incidence wide-angle X-ray scattering (2D-GIWAXS). From the 2D GIWAXS patterns and 1D line-cut profiles of BSS*x*:PBDB-T blends (Figure 4) and the neat BSS*x* copolymers (Figure S12), we found that the neat BSS*x* (x = 10, 20, 50) acceptors had enhanced *face-on* molecular orientation compared to BSS0 based on the intensities of the (010) π- π stacking peaks in the out-of-plane (OOP) direction. This is in good agreement with measured SCLC electron mobilities (Table S4). The crystal coherence length (CCL) calculated using the Scherrer equation analysis of the (100) lamellar peak in the in-plane (IP) direction was 9.7-10.7 nm in the random copolymers compared to 11.6 nm in the reference BSS0. The GIWAXS results show that the random copolymers BSS*x* combine reduced crystallinity with enhanced *face-on* ordering, which could help to achieve compatible blends with favorable morphology when mixed with less crystalline PBDB-T donor (CCL = 1.3 nm).

In the BSS*x*:PBDB-T blend films, the presence of a (100) peak (q_{xy} = 0.27 Å^{-1}) along the IP direction and a (010) peak (q_z = 1.65 – 1.69 Å^{-1}) along the OOP direction (Figure 4) confirmed the preferential *face-on* molecular orientation. The lower diffraction peak intensities and the

smaller CCL (Table S5) as a function of selenophene composition suggest that the crystallinity and domain sizes are significantly reduce in BSS*x* (*x* = 10, 20, 50) blend films. Overall, the 2D GIWAXS results show that the BSS10 copolymer with optimal crystallinity exhibited favorable morphology, which agrees well with the observed high J_{sc}, FF, and PCE in the BSS*x*-based all-PSCs.

In summary, we have synthesized a series of new n-type semiconducting random copolymers BSS*x* (*x* = 10, 20, 50) and investigated them as the acceptor component in all-PSCs in comparison with the reference BSS0. Blends of each BSS*x* with donor polymer PBDB-T could produce high efficiency (>9.6%) all-PSCs without use of a solution processing additive. All-polymer solar cells that combine high efficiency (>10%) with nearly 100% internal quantum efficiency and small optical bandgap energy loss (<0.6 eV) have been developed from the new random copolymer acceptor BSS10 with optimum composition. Furthermore, all-PSCs produced from BSS10 and BSS20 had high external quantum efficiencies (>85%) and small E_{loss} (<0.6 eV), the best combination yet found for all-PSCs. The observed enhanced performance in photovoltaic devices composed of BSS*x* random copolymer and PBDB-T relative to BSS0:PBDB-T blends originates from the optimal morphology enabled by the preferential *face-on* molecular packing and reduced crystalline domain size in BSS*x*. The results of this work demonstrate that random copolymer architectures are promising molecular design strategies for optimizing the morphology and increasing the performance of all-PSCs.

ASSOCIATED CONTENT

Supporting Information

The Supporting Information is available free of charge on the ACS Publication website at DOI:

Synthesis details, ^{1}H NMR, TGA, DSC, UV-Vis, CV characterization, and all-PSC device fabrication and characterization, additional *J-V* characteristics, SCLC mobility measurement, morphology characterization via AFM and 2D-GIWAXS

AUTHOR INFORMATION

Corresponding Author

*Email: jenekhe@u.wahington.edu

Author Contributions

‡ These authors contributed equally.

Notes

The authors declare no competing financial interest.

ACKNOWLEDGEMENTS

This work was supported by the Office of Naval Research (N00014-17-1-2203) and in part by the NSF (DMR-1708450). The synchrotron radiation based 2D-GIWAXS experiments were performed at the BL46XU and BL19B2 of SPring-8 with the approval of the Japan Synchrotron Radiation Research Institute (JASRI) (Proposal No. 2018A1744 and 2018B1772). We thank Tosoh Bioscience (USA) for high temperature GPC molecular weight characterization of the polymers.

REFERENCES

(1) Zhang, G.; Zhao, J.; Chow, P. C. Y.; Jiang, K.; Zhang, J.; Zhu, Z.; Zhang, J.; Huang, F.; Yan, H. Nonfullerene Acceptor Molecules for Bulk Heterojunction Organic Solar Cells. *Chem. Rev.* **2018,** *118* (7), 3447-3507.

(2) Yan, C.; Barlow, S.; Wang, Z.; Yan, H.; Jen, A. K. Y.; Marder, S. R.; Zhan, X. Non-fullerene acceptors for organic solar cells. *Nat. Rev. Mater.* **2018,** *3* (3), 18003.

(3) Li, H.; Earmme, T.; Ren, G.; Saeki, A.; Yoshikawa, S.; Murari, N. M.; Subramaniyan, S.; Crane, M. J.; Seki, S.; Jenekhe, S. A. Beyond Fullerenes: Design of

Nonfullerene Acceptors for Efficient Organic Photovoltaics. *J. Am. Chem. Soc.* **2014,** *136* (41), 14589-14597.

(4) Hwang, Y.-J.; Li, H.; Courtright, B. A. E.; Subramaniyan, S.; Jenekhe, S. A. Nonfullerene Polymer Solar Cells with 8.5% Efficiency Enabled by a New Highly Twisted Electron Acceptor Dimer. *Adv. Mater.* **2016,** *28* (1), 124-131.

(5) Wang, W.; Zhao, B.; Cong, Z.; Xie, Y.; Wu, H.; Liang, Q.; Liu, S.; Liu, F.; Gao, C.; Wu, H.; Cao, Y. Nonfullerene Polymer Solar Cells Based on a Main-Chain Twisted Low-Bandgap Acceptor with Power Conversion Efficiency of 13.2%. *ACS Energy Lett.* **2018,** *3* (7), 1499-1507.

(6) Yuan, J.; Zhang, Y.; Zhou, L.; Zhang, G.; Yip, H.-L.; Lau, T.-K.; Lu, X.; Zhu, C.; Peng, H.; Johnson, P. A.; Leclerc, M.; Cao, Y.; Ulanski, J.; Li, Y.; Zou, Y. Single-Junction Organic Solar Cell with over 15% Efficiency Using Fused-Ring Acceptor with Electron-Deficient Core. *Joule* **2019,** *3*, 1-12.

(7) Meng, L.; Zhang, Y.; Wan, X.; Li, C.; Zhang, X.; Wang, Y.; Ke, X.; Xiao, Z.; Ding, L.; Xia, R.; Yip, H.-L.; Cao, Y.; Chen, Y. Organic and solution-processed tandem solar cells with 17.3% efficiency. *Science* **2018,** *361* (6407), 1094-1098.

(8) Wang, G.; Melkonyan, F. S.; Facchetti, A.; Marks, T. J. All-Polymer Solar Cells: Recent Progress, Challenges, and Prospects. *Angew. Chem. Int. Ed.* **2018,** DOI:10.1002/anie.201808976.

(9) Benten, H.; Mori, D.; Ohkita, H.; Ito, S. Recent research progress of polymer donor/polymer acceptor blend solar cells. *J. Mater. Chem. A* **2016,** *4* (15), 5340-5365.

(10) Genene, Z.; Mammo, W.; Wang, E.; Andersson, M. R. Recent Advances in n-Type Polymers for All-Polymer Solar Cells. *Adv. Mater.* **2019,** DOI:10.1002/adma.201807275.

(11) Liu, Z.; Zeng, D.; Gao, X.; Li, P.; Zhang, Q.; Peng, X. Non-fullerene polymer acceptors based on perylene diimides in all-polymer solar cells. *Sol. Energy Mater Sol. Cells* **2019,** *189*, 103-117.

(12) Hwang, Y.-J.; Courtright, B. A. E.; Ferreira, A. S.; Tolbert, S. H.; Jenekhe, S. A. 7.7% Efficient All-Polymer Solar Cells. *Adv. Mater.* **2015,** *27* (31), 4578-4584.

(13) Gao, L.; Zhang, Z. G.; Xue, L.; Min, J.; Zhang, J.; Wei, Z.; Li, Y. All-Polymer Solar Cells Based on Absorption-Complementary Polymer Donor and Acceptor with High Power Conversion Efficiency of 8.27%. *Adv. Mater.* **2016,** *28* (9), 1884-1890.

(14) Fan, B.; Ying, L.; Zhu, P.; Pan, F.; Liu, F.; Chen, J.; Huang, F.; Cao, Y. All-Polymer Solar Cells Based on a Conjugated Polymer Containing Siloxane-Functionalized Side Chains with Efficiency over 10%. *Adv. Mater.* **2017,** *29* (47), 1703906.

(15) Fan, B.; Ying, L.; Wang, Z.; He, B.; Jiang, X.-F.; Huang, F.; Cao, Y. Optimisation of processing solvent and molecular weight for the production of green-solvent-processed all-polymer solar cells with a power conversion efficiency over 9%. *Energy Environ. Sci.* **2017,** *10* (5), 1243-1251.

(16) Li, Z.; Xu, X.; Zhang, W.; Meng, X.; Genene, Z.; Ma, W.; Mammo, W.; Yartsev, A.; Andersson, M. R.; Janssen, R. A. J.; Wang, E. 9.0% power conversion efficiency from ternary all-polymer solar cells. *Energy Environ. Sci.* **2017,** *10* (10), 2212-2221.

(17) Guo, Y.; Li, Y.; Awartani, O.; Han, H.; Zhao, J.; Ade, H.; Yan, H.; Zhao, D. Improved Performance of All-Polymer Solar Cells Enabled by Naphthodiperylenetetraimide-Based Polymer Acceptor. *Adv. Mater.* **2017,** *29* (26), 1700309.

(18) Kolhe, N. B.; Lee, H.; Kuzuhara, D.; Yoshimoto, N.; Koganezawa, T.; Jenekhe, S. A. All-Polymer Solar Cells with 9.4% Efficiency from Naphthalene Diimide-Biselenophene Copolymer Acceptor. *Chem. Mater.* **2018,** *30* (18), 6540-6548.

(19) Yao, H.; Bai, F.; Hu, H.; Arunagiri, L.; Zhang, J.; Chen, Y.; Yu, H.; Chen, S.; Liu, T.; Lai, J. Y. L.; Zou, Y.; Ade, H.; Yan, H. Efficient All-Polymer Solar Cells based on a New Polymer Acceptor Achieving 10.3% Power Conversion Efficiency. *ACS Energy Lett.* **2019,** *4* (2), 417-422.

(20) Liu, X.; Zhang, C.; Duan, C.; Li, M.; Hu, Z.; Wang, J.; Liu, F.; Li, N.; Brabec, C. J.; Janssen, R. A. J.; Bazan, G. C.; Huang, F.; Cao, Y. Morphology Optimization via Side Chain Engineering Enables All-Polymer Solar Cells with Excellent Fill Factor and Stability. *J. Am. Chem. Soc.* **2018,** *140* (28), 8934-8943.

(21) Lin, Y.; Dong, S.; Li, Z.; Zheng, W.; Yang, J.; Liu, A.; Cai, W.; Liu, F.; Jiang, Y.; Russell, T. P.; Huang, F.; Wang, E.; Hou, L. Energy-effectively printed all-polymer solar cells exceeding 8.61% efficiency. *Nano Energy* **2018,** *46*, 428-435.

(22) Zhang, Z.-G.; Yang, Y.; Yao, J.; Xue, L.; Chen, S.; Li, X.; Morrison, W.; Yang, C.; Li, Y. Constructing a Strongly Absorbing Low-Bandgap Polymer Acceptor for High-Performance All-Polymer Solar Cells. *Angew. Chem. Int. Ed.* **2017,** *56* (43), 13503-13507.

(23) Chen, D.; Yao, J.; Chen, L.; Yin, J.; Lv, R.; Huang, B.; Liu, S.; Zhang, Z.-G.; Yang, C.; Chen, Y.; Li, Y. Dye-Incorporated Polynaphthalenediimide Acceptor for Additive-Free High-Performance All-Polymer Solar Cells. *Angew. Chem. Int. Ed.* **2018,** *57* (17), 4580-4584.

(24) Hwang, Y.-J.; Earmme, T.; Courtright, B. A. E.; Eberle, F. N.; Jenekhe, S. A. n-Type Semiconducting Naphthalene Diimide-Perylene Diimide Copolymers: Controlling Crystallinity,

Blend Morphology, and Compatibility Toward High-Performance All-Polymer Solar Cells. *J. Am. Chem. Soc.* **2015,** *137* (13), 4424-4434.

(25) Jackson, N. E.; Savoie, B. M.; Marks, T. J.; Chen, L. X.; Ratner, M. A. The Next Breakthrough for Organic Photovoltaics? *J. Phys. Chem. Lett.* **2015,** *6* (1), 77-84.

(26) Wang, G.; Eastham, N. D.; Aldrich, T. J.; Ma, B.; Manley, E. F.; Chen, Z.; Chen, L. X.; de la Cruz, M. O.; Chang, R. P. H.; Melkonyan, F. S.; Facchetti, A.; Marks, T. J. Photoactive Blend Morphology Engineering through Systematically Tuning Aggregation in All-Polymer Solar Cells. *Adv. Energy Mater.* **2018,** *8* (12), 1702173.

(27) Kang, H.; Lee, W.; Oh, J.; Kim, T.; Lee, C.; Kim, B. J., From Fullerene–Polymer to All-Polymer Solar Cells: The Importance of Molecular Packing, Orientation, and Morphology Control. *Acc. Chem. Res.* **2016,** *49* (11), 2424-2434.

(28) Ye, L.; Jiao, X.; Zhao, W.; Zhang, S.; Yao, H.; Li, S.; Ade, H.; Hou, J. Manipulation of Domain Purity and Orientational Ordering in High Performance All-Polymer Solar Cells. *Chem. Mater.* **2016,** *28* (17), 6178-6185.

(29) Yuan, J.; Xu, Y.; Shi, G.; Ling, X.; Ying, L.; Huang, F.; Lee, T. H.; Woo, H. Y.; Kim, J. Y.; Cao, Y.; Ma, W. Engineering the morphology via processing additives in multiple all-polymer solar cells for improved performance. *J. Mater. Chem. A* **2018,** *6* (22), 10421-10432.

(30) Shi, G.; Yuan, J.; Huang, X.; Lu, Y.; Liu, Z.; Peng, J.; Ding, G.; Shi, S.; Sun, J.; Lu, K.; Wang, H.-Q.; Ma, W. Combinative Effect of Additive and Thermal Annealing Processes Delivers High Efficiency All-Polymer Solar Cells. *J. Phys. Chem. C* **2015,** *119* (45), 25298-25306.

(31) Kim, Y. J.; Ahn, S.; Wang, D. H.; Park, C. E. A Mechanistic Understanding of a Binary Additive System to Synergistically Boost Efficiency in All-Polymer Solar Cells. *Scientific Reports* **2015,** *5*, 18024.

(32) Earmme, T.; Hwang, Y.-J.; Murari, N. M.; Subramaniyan, S.; Jenekhe, S. A. All-Polymer Solar Cells with 3.3% Efficiency Based on Naphthalene Diimide-Selenophene Copolymer Acceptor. *J. Am. Chem. Soc.* **2013,** *135* (40), 14960-14963.

(33) Lee, W.; Lee, C.; Yu, H.; Kim, D.-J.; Wang, C.; Woo, H. Y.; Oh, J. H.; Kim, B. J. Side Chain Optimization of Naphthalenediimide–Bithiophene-Based Polymers to Enhance the Electron Mobility and the Performance in All-Polymer Solar Cells. *Adv. Funct. Mater.* **2016,** *26* (10), 1543-1553.

(34) Hwang, Y. J.; Earmme, T.; Subramaniyan, S.; Jenekhe, S. A. Side chain engineering of n-type conjugated polymer enhances photocurrent and efficiency of all-polymer solar cells. *Chem. Commun.* **2014,** *50* (74), 10801-4.

(35) Earmme, T.; Hwang, Y.-J.; Subramaniyan, S.; Jenekhe, S. A. All-Polymer Bulk Heterojuction Solar Cells with 4.8% Efficiency Achieved by Solution Processing from a Co-Solvent. *Adv. Mater.* **2014,** *26* (35), 6080-6085.

(36) Li, Z.; Xu, X.; Zhang, W.; Meng, X.; Ma, W.; Yartsev, A.; Inganäs, O.; Andersson, M. R.; Janssen, R. A. J.; Wang, E. High Performance All-Polymer Solar Cells by Synergistic Effects of Fine-Tuned Crystallinity and Solvent Annealing. *J. Am. Chem. Soc.* **2016,** *138* (34), 10935-10944.

(37) Sharma, S.; Kolhe, N. B.; Gupta, V.; Bharti, V.; Sharma, A.; Datt, R.; Chand, S.; Asha, S. K. Improved All-Polymer Solar Cell Performance of n-Type Naphthalene Diimide–

Bithiophene P(NDI2OD-T2) Copolymer by Incorporation of Perylene Diimide as Coacceptor. *Macromolecules* **2016,** *49* (21), 8113-8125.

(38) Li, Z.; Xu, X.; Zhang, W.; Meng, X.; Ma, W.; Yartsev, A.; Inganas, O.; Andersson, M. R.; Janssen, R. A.; Wang, E. High Performance All-Polymer Solar Cells by Synergistic Effects of Fine-Tuned Crystallinity and Solvent Annealing. *J. Am. Chem. Soc.* **2016,** *138* (34), 10935-44.

(39) Kim, Y.; Cho, H.-H.; Kim, T.; Liao, K.; Kim, B. J. Terpolymer approach for controlling the crystalline behavior of naphthalene diimide-based polymer acceptors and enhancing the performance of all-polymer solar cells. *Polym. J.* **2016,** *48* (4), 517-524.

(40) Dang, D.; Yu, D.; Wang, E. Conjugated Donor-Acceptor Terpolymers Toward High-Efficiency Polymer Solar Cells. *Adv. Mater.* **2019,** DOI:10.1002/adma.201807019.

(41) Hwang, Y.-J.; Ren, G.; Murari, N. M.; Jenekhe, S. A. n-Type Naphthalene Diimide–Biselenophene Copolymer for All-Polymer Bulk Heterojunction Solar Cells. *Macromolecules* **2012,** *45* (22), 9056-9062.

(42) Hwang, Y.-J.; Murari, N. M.; Jenekhe, S. A. New n-type polymer semiconductors based on naphthalene diimide and selenophene derivatives for organic field-effect transistors. *Polym. Chem.* **2013,** *4* (11), 3187-3195.

(43) Ren, G.; Schlenker, C. W.; Ahmed, E.; Subramaniyan, S.; Olthof, S.; Kahn, A.; Ginger, D. S.; Jenekhe, S. A. Photoinduced Hole Transfer Becomes Suppressed with Diminished Driving Force in Polymer-Fullerene Solar Cells While Electron Transfer Remains Active. *Adv. Funct. Mater.* **2013,** *23* (10), 1238-1249.

(44) Li, H.; Hwang, Y.-J.; Earmme, T.; Huber, R. C.; Courtright, B. A. E.; O'Brien, C.; Tolbert, S. H.; Jenekhe, S. A. Polymer/Polymer Blend Solar Cells Using

Tetraazabenzodifluoranthene Diimide Conjugated Polymers as Electron Acceptors. *Macromolecules* **2015,** *48* (6), 1759-1766.

(45) Gao, L.; Zhang, Z.-G.; Xue, L.; Min, J.; Zhang, J.; Wei, Z.; Li, Y. All-Polymer Solar Cells Based on Absorption-Complementary Polymer Donor and Acceptor with High Power Conversion Efficiency of 8.27%. *Adv. Mater.* **2016,** *28* (9), 1884-1890.

(46) Zhou, N.; Lin, H.; Lou, S. J.; Yu, X.; Guo, P.; Manley, E. F.; Loser, S.; Hartnett, P.; Huang, H.; Wasielewski, M. R.; Chen, L. X.; Chang, R. P. H.; Facchetti, A.; Marks, T. J. Morphology-Performance Relationships in High-Efficiency All-Polymer Solar Cells. *Adv. Energy Mater.* **2014,** *4* (3), 1300785.

(47) Xu, X.; Li, Z.; Wang, J.; Lin, B.; Ma, W.; Xia, Y.; Andersson, M. R.; Janssen, R. A. J.; Wang, E. High-performance all-polymer solar cells based on fluorinated naphthalene diimide acceptor polymers with fine-tuned crystallinity and enhanced dielectric constants. *Nano Energy* **2018,** *45*, 368-379.

(48) Duan, C.; Li, Z.; Pang, S.; Zhu, Y.-L.; Lin, B.; Colberts, F. J. M.; Leenaers, P. J.; Wang, E.; Sun, Z.-Y.; Ma, W.; Meskers, S. C. J.; Janssen, R. A. J. Improving Performance of All-Polymer Solar Cells Through Backbone Engineering of Both Donors and Acceptors. *Sol. RRL* **2018,** *2* (12), 1800247.

(49) Sun, H.; Tang, Y.; Guo, H.; Uddin, M. A.; Ling, S.; Wang, R.; Wang, Y.; Zhou, X.; Woo, H. Y.; Guo, X. Fluorine Substituted Bithiophene Imide-Based n-Type Polymer Semiconductor for High-Performance Organic Thin-Film Transistors and All-Polymer Solar Cells. *Sol. RRL* **2019,** *3* (2), 1800265.

(50) Li, Z.; Ying, L.; Zhu, P.; Zhong, W.; Li, N.; Liu, F.; Huang, F.; Cao, Y. A generic green solvent concept boosting the power conversion efficiency of all-polymer solar cells to 11%. *Energy Environ. Sci.* **2019,** *12* (1), 157-163.

(51) You, H.; Kim, D.; Cho, H.-H.; Lee, C.; Chong, S.; Ahn, N. Y.; Seo, M.; Kim, J.; Kim, F. S.; Kim, B. J. Shift of the Branching Point of the Side-Chain in Naphthalenediimide (NDI)-Based Polymer for Enhanced Electron Mobility and All-Polymer Solar Cell Performance. *Adv. Funct. Mater.* **2018,** *28* (39), 1803613.

(52) Cho, H.-H.; Kim, T.; Kim, K.; Lee, C.; Kim, F. S.; Kim, B. J. Synthesis and side-chain engineering of phenylnaphthalenediimide (PNDI)-based n-type polymers for efficient all-polymer solar cells. *J. Mater. Chem. A* **2017,** *5* (11), 5449-5459.

(53) Courtright, B. A. E.; Jenekhe, S. A. Polyethylenimine Interfacial Layers in Inverted Organic Photovoltaic Devices: Effects of Ethoxylation and Molecular Weight on Efficiency and Temporal Stability. *ACS Appl. Mater. Interfaces* **2015,** *7* (47), 26167-26175.

(54) Peet, J.; Kim, J. Y.; Coates, N. E.; Ma, W. L.; Moses, D.; Heeger, A. J.; Bazan, G. C. Efficiency Enhancement in Low-Bandgap Polymer Solar Cells by Processing with Alkane Dithiols. *Nat. Mater.* **2007,** *6*, 497.

(55) Li, W.; Hendriks, K. H.; Furlan, A.; Wienk, M. M.; Janssen, R. A. High quantum efficiencies in polymer solar cells at energy losses below 0.6 eV. *J. Am. Chem. Soc.* **2015,** *137* (6), 2231-4.

(56) Menke, S. M.; Ran, N. A.; Bazan, G. C.; Friend, R. H., Understanding Energy Loss in Organic Solar Cells: Toward a New Efficiency Regime. *Joule* **2018**, 2 (1), 25-35.

(57) Azzouzi, M.; Kirchartz, T.; Nelson, J., Factors Controlling Open-Circuit Voltage Losses in Organic Solar Cells. *Trends in Chemistry* **2019**, 1 (1), 49-62.

(58) Burkhard, G. F.; Hoke, E. T.; McGehee, M. D. Accounting for Interference, Scattering, and Electrode Absorption to Make Accurate Internal Quantum Efficiency Measurements in Organic and Other Thin Solar Cells. *Adv. Mater.* **2010,** *22* (30), 3293-3297.

(59) Park, S. H.; Roy, A.; Beaupré, S.; Cho, S.; Coates, N.; Moon, J. S.; Moses, D.; Leclerc, M.; Lee, K.; Heeger, A. J. Bulk heterojunction solar cells with internal quantum efficiency approaching 100%. *Nat. Photon.* **2009,** *3* (5), 297-302.

(60) Mori, D.; Benten, H.; Okada, I.; Ohkita, H.; Ito, S. Highly efficient charge-carrier generation and collection in polymer/polymer blend solar cells with a power conversion efficiency of 5.7%. *Energy Environ. Sci.* **2014,** *7* (9), 2939-2943.

(61) Schilinsky, P.; Waldauf, C.; Brabec, C. J. Recombination and loss analysis in polythiophene based bulk heterojunction photodetectors. *Appl.Phys. Lett.* **2002,** *81* (20), 3885-3887.

(62) Proctor, C. M.; Kuik, M.; Nguyen, T.-Q. Charge carrier recombination in organic solar cells. *Prog. Polym. Sci.* **2013,** *38* (12), 1941-1960.

Supporting Information for

New Random Copolymer Acceptors Enable Additive-Free Processing of 10.1% Efficient All-Polymer Solar Cells with Near Unity Internal Quantum Efficiency

Nagesh B. Kolhe, [†] Duyen K. Tran, [†] Hyunjong Lee, [†] Daiki Kuzuhara, [§] Noriyuki Yoshimoto, [§] Tomoyuki Koganezawa,[‖] and Samson A. Jenekhe*,[†]

[†]Department of Chemical Engineering and Department of Chemistry, University of Washington, Seattle, Washington 98195-1750, USA

[§]Faculty of Science and Engineering, Iwate University, 4-3-5 Ueda, Morioka, Iwate, 020-8551, Japan

[‖]Industrial Application Division, Japan Synchrotron Radiation Research Institute, Sayo, Hyogo, 679-5198, Japan

Table of Contents

EXPERIMENTAL METHODS

Materials. Tri-(*o*-tolyl)-phosphine, tris(dibenzylideneacetone)dipalladium (0) ($Pd_2(dba)_3$), selenophene, trimethyltin chloride (20% solution) in THF, anhydrous copper(II)chloride, *n*-butyl lithium (2M in hexane), and chlorobenzene were purchased from Sigma-Aldrich and used without further purification. 5,10-Dibromoisochromeno[6,5,4-*def*] isochromene-1,3,6,8(*3aH, 8aH*)-tetraone and 2-octyldodecyl amine were purchased from Suna Tech Inc (Jaiansu, China). The donor polymer PBDB-T (M_n = 62 kDa, $Đ$ = 1.90) was purchased from Brilliant Matters Organic electronics (Quebec, Canada) and used as received.

Synthesis.

Monomer Synthesis. 5,5′-bis (trimethylstannyl)-2,2'-biselenophene, 2,5-bis (trimethylstannyl)-selenophene and 4,9-dibromo-2,7-bis(2-octyldodecyl) benzo[lmn][3,8]phenanthroline-1,3,6,8-tetraone monomers were synthesized according to our previously reported procedures. [1, 2]

Synthesis of [Poly {[*N*,*N*′-bis(2-octyldodecyl)-naphthalene-1,4,5,8-bis(dicarboximide)-2,6-diyl]-*alt*-5,5′-(2,2'-biselenophene)}-*ran*-{[*N*,*N*′-bis(2-octyldodecyl)-naphthalene-1,4,5,8 bis(dicarboximide)-2,6-diyl]-*alt*-5,5′-(selenophene)] (BSS*x*).

Scheme 1. Synthetic Route to Random Copolymer Acceptors (BSS*x*).

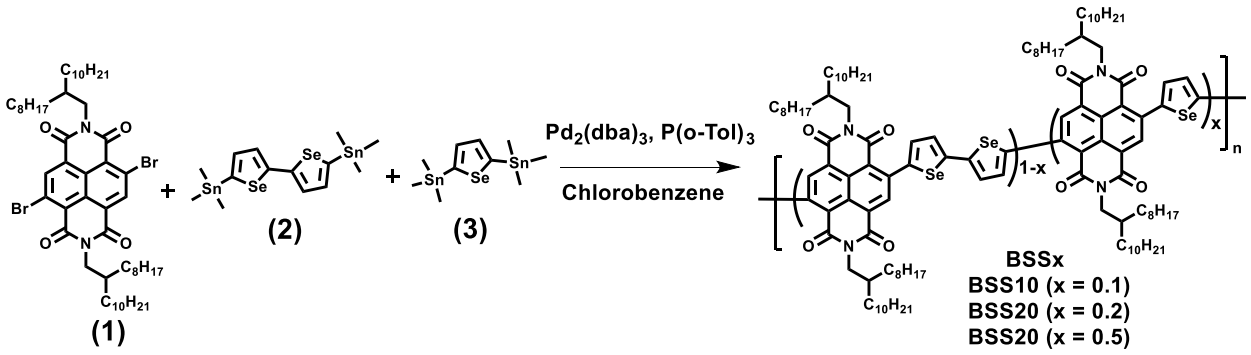

Copolymer BSS10

4,9-Dibromo-2,7-bis(2-octyldodecyl) benzo[lmn] [3,8] phenanthroline-1,3,6,8-tetraone , **1** (550 mg, 0.558 mmol), 5,5'-bis(trimethylstannyl)-2,2'biselenophene, **2** (294 mg, 0.502 mmol), 2,5-bis (trimethylstannyl)-selenophene , **3** (26 mg, 0.055 mmol), $Pd_2(dba)_3$ (20 mg, 3.5 mole%) and P(*o*-tolyl)$_3$ (32.5 mg) were added into a 100-mL air free Schlenk tube and then degassed and filled with argon three times. Afterwards, 25 mL chlorobenzene was added and degassed and filled with argon three times. The reaction mixture was stirred at 120 °C for 4 days under argon. The reaction mixture was cooled to 100 °C and (0.1 mL) trimethytinbenzene was added and stirred for 12 hours followed by addition of (0.1mL) bromobenzene and stirring for another 12 hours to complete the polymer end-capping. After cooling down to room temperature, the polymerization mixture was poured into 500 mL methanol/ 10 mL hydrochloric acid solution and stirred for 3 h. The polymer precipitated out as a bluish green solid and was filtered using a buchner funnel. The polymer was purified by Soxhlet extraction sequentially with methanol, acetone, and hexane, and subsequently extracted in hot chloroform for 3h. The chloroform was concentrated and precipitated in 400 mL methanol to give BSS10**.** Yield, 560 mg, 93 %.

Copolymer BSS20

It was synthesized by using similar procedure as mentioned above, starting with **1** (500 mg, 0.507 mmol), **2** (237 mg, 0.406 mmol), **3** (47 mg, 0.101mmol), $Pd_2(dba)_3$ (20 mg, 3.5 mole%) and P(*o*-tolyl)$_3$ (32.5 mg). Yield, 520 mg, 95%.

Copolymer BSS50

It was synthesized by using similar procedure as mentioned above, starting with **1** (500 mg, 0.507 mmol), **2** (148 mg, 0.253 mmol), **3** (115 mg, 0.0.253mmol), $Pd_2(dba)_3$ (20 mg, 3.5 mole%) and P(*o*-tolyl)$_3$ (32.5 mg). Yield, 450 mg, 75%.

Characterizations

^{1}H NMR spectra were recorded on a Bruker AV500 at 500 MHz using deuterated chloroform ($CDCl_3$) as the solvent at 329 K. Size exclusion chromatography (SEC) analysis was performed using EcoSEC High temperature GPC system (HLC-8321GPC/HT) against polystyrene standards in chlorobenzene 1,2,3-trichlorobenzene at 120 °C (flow rate 1mL/min). Thermogravimetric analysis (TGA) of the polymers was conducted on a TA Instrument model Q50TGA. A heating rate of 10 °C /min under a flow of N_2 was used with runs conducted from room temperature to 850 °C. Differential scanning calorimetry (DSC) analysis was performed on a TA Instruments Q100 under N_2 by scanning from -10 °C to 370 °C at a heating rate and cooling rate of 10 °C /min. Optical absorption spectra of the polymers were measured on a PerkinElmer model Lambda 900 UV-vis/near-IR spectrophotometer. Solution and solid-state absorption spectra were obtained from dilute (10^{-6} M) polymer solution in chloroform and from thin films on glass substrate, respectively. Thin films were spin coated from 20 mg/mL solutions in chlorobenzene. Photoluminescence (PL) measurements were carried out with a Photon Technology International (PTI) Inc. model QM2001-4 spectrofluorimeter using xenon flash lamp as the light source.

Cyclic voltammetry (CV) experiments were done on an EG&G Princeton Applied Research potentiostat/galvanostat (model 273A). A three-electrode cell was used, using platinum wire electrodes as both counter and working electrode. Silver/silver ion (Ag in 0.1 M $AgNO_3$ solution) was used as a reference electrode. Films of the random copolymers were coated onto the

Pt wires by dipping the wires into the copolymer solutions in chloroform then drying the coated films at 25 °C. All the CV measurements were carried out in 0.1 M tetrabutylammonium hexafluorophosphate (Bu_4NPF_6) electrolyte solution in acetonitrile at a scan rate of 50 mV/s. The reduction and oxidation potentials were referenced to the Fc/Fc^+ couple by using ferrocene as an internal standard. LUMO energy levels were estimated using ferrocene value of -4.8 eV with respect to vacuum level. The LUMO and HOMO levels were determined by using equation $E_{LUMO} = -(eE_{red}^{onset} + 4.8)$ and $E_{HOMO} = -(eE_{ox}^{onset}+4.8)$, respectively.

Atomic force microscopy (AFM) characterization of the surface morphology was done, using a Bruker Dimension scanning probe microscope (SPM) system, on the active layers of actual all-PSC devices.

Grazing incidence X-ray scattering (GIWAXS) experiments were conducted at the Japan Synchrotron Radiation Facility SPring-8 by using the beamlines BL46XU and BL19B2. Thin-film samples of the neat acceptor polymers (BSS*x*) and donor polymer PBDB-T were spin-coated on glass substrates and annealed at 175 °C for 10 min, and the films of BSS*x*:PBDB-T blends were prepared in the same manner as the actual all-PSC devices on ZnO-coated ITO substrates. The X-ray beam was monochromatized by a double-crystal Si (111) monochromator and the X-ray energy in this experiment was 12.40 keV (λ = 0.1 nm). The angle of incident X-ray to sample surface was 0.12º with a Huber diffractometer. The scattered profile from the film sample was detected using an area detector (PILATUS 300K) for 1 s at room temperature and the distance between the sample and detector was 174.0 mm. The crystal coherence length (L_c) of samples were analyzed by using the Scherrer equation: $Lc = 2\pi K / \Delta q$, where K is a shape factor (typically 0.89), and Δq is the full width at half maxima (FWHM) of the diffraction peak. Here, the $L_c^{(100)}$ was obtained from the FWHM of the (100) diffraction peak in the-plane (q_{xy}) line cut.

Fabrication and characterization of Polymer Solar Cells.

All-polymer solar cells were fabricated with an inverted architecture of ITO/ZnO/PEI/Blend/MoO_3/Ag. ITO-coated substrates (15 Ω /square, Shanghai B. Tree Tech, Shanghai, China) were cleaned sequentially in ultrasonic baths with acetone, deionized water, and isopropyl alcohol for 30 min, dried using nitrogen gas, and followed by 90 s of O_2 plasma cleaning. The ZnO precursor solution was spin-coated onto the ITO substrates at 5000 rpm for 40 s, followed by thermal annealing at 250 °C for 30 min to make ~30 nm thick ZnO layer. A 0.05 wt% solution of polyethylenimine (PEI, $M_w \approx 25\,000$, Aldrich 408727) in 2-methoxyethanol was spin-coated onto the ZnO layer and dried at 120 °C for 10 min. The solution for each BSS*x*:PBDB-T blend (0.6:1 wt/wt) was prepared in chlorobenzene, mixed and stirred overnight at 80 °C in the glove box. The blend solution was spin-coated at 1000 rpm for 50 s, followed by thermal annealing at 175 °C for 10 min in the glove box. All the active layers had a thickness of 90 ± 10 nm. MoO_3 (0.5 nm) and Ag (100 nm) were thermally deposited onto the active layer. Each substrate contained four devices, each with an active area of 9 mm^2. An aperture mask with area of 3.14 mm^2 is applied during measurements to define the illuminated device area. After evaporation of the electrode, the photovoltaic cells were tested under AM 1.5G solar illumination at 100 mW/cm^2 in ambient air by using a solar simulator (Model 16S, Solar Light Co., Philadelphia, PA) with a 200W Xenon Lamp Power Supply (Model XPS 200, Solar Light Co., Philadelphia, PA) calibrated by NREL certified Si photodiode (Model 1787-04, Hamamatsu Photonics K.K., Japan) and a HP4155A semiconductor parameter analyzer (Yokogawa Hewlett Packard, Japan). After the *J-V* measurement, the external quantum efficiency (EQE), internal quantum efficiency (IQE), and reflectance spectra were measured by using a solar cell quantum efficiency measurement system (Model QEX10, PV Measurements, Inc., Boulder, CO) with a 2 mm^2 (2 mm × 1 mm) size masked incident light source and TF Mini Super measurement apparatus for multiple devices in a single

substrate. The EQE and IQE system was calibrated with a Si photodiode before measurement. The reflectance spectra were measured on actual solar cell devices by an integrating sphere to fully account for possible interference from the reflective electrodes; thus, ensuring high accuracy IQE measurements. The internal quantum efficiency (IQE) was obtained by normalizing the EQE spectra to the reflectance spectra.

Fabrication and Characterization of SCLC devices

Current-voltage (*J-V*) characteristics of the SCLC devices were measured by using a HP4155A semiconductor parameter analyzer (Yokogawa Hewlett-Packard, Tokyo). The carrier mobility was deduced by fitting the *J-V* curves to the Mott−Gurney equation where *J* is the current density, ε_0 is the permittivity of free space, ε is the relative permittivity, μ is the zero-field mobility, *V* is the applied voltage, *d* is the thickness of active layer.

$$J = \frac{9}{8}\varepsilon\varepsilon_0\mu\frac{V^2}{d^3}$$

The SCLC device structures for electron-only and hole-only were ITO/ZnO/PEI/Blend/LiF (2nm)/Al (100nm) and ITO/PEDOT: PSS/Blend/MoO_3 (7.5nm)/Ag (100nm), respectively. Each active layer, which was comprised of chlorobenzene solutions of PBDB-T and acceptor polymers (BSS*x*) at D/A ratio of 1 to 0.6, was spin-coated at 1000 rpm for 50s and followed by thermal annealing at 175°C for 10 min inside glovebox. All active layers had thickness of 175 ± 10 nm.

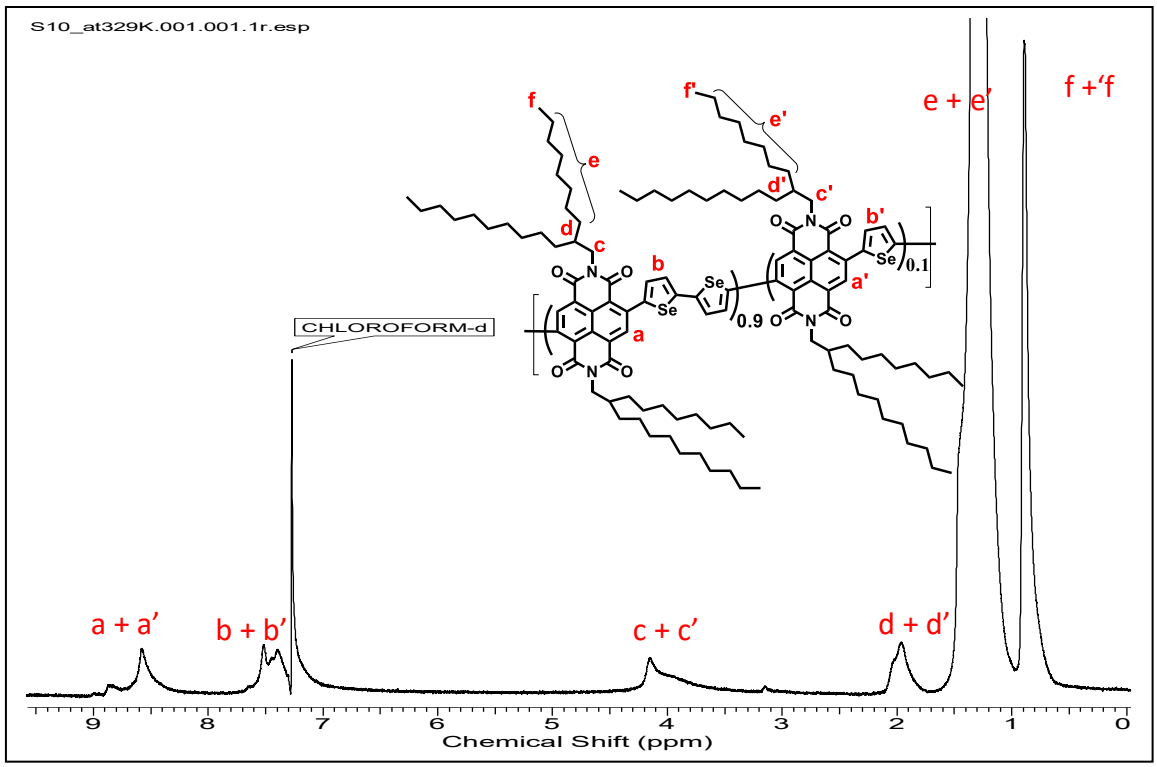

Figure S1a. ^{1}H NMR spectrum of BSS10 in $CDCl_3$ at 329K.

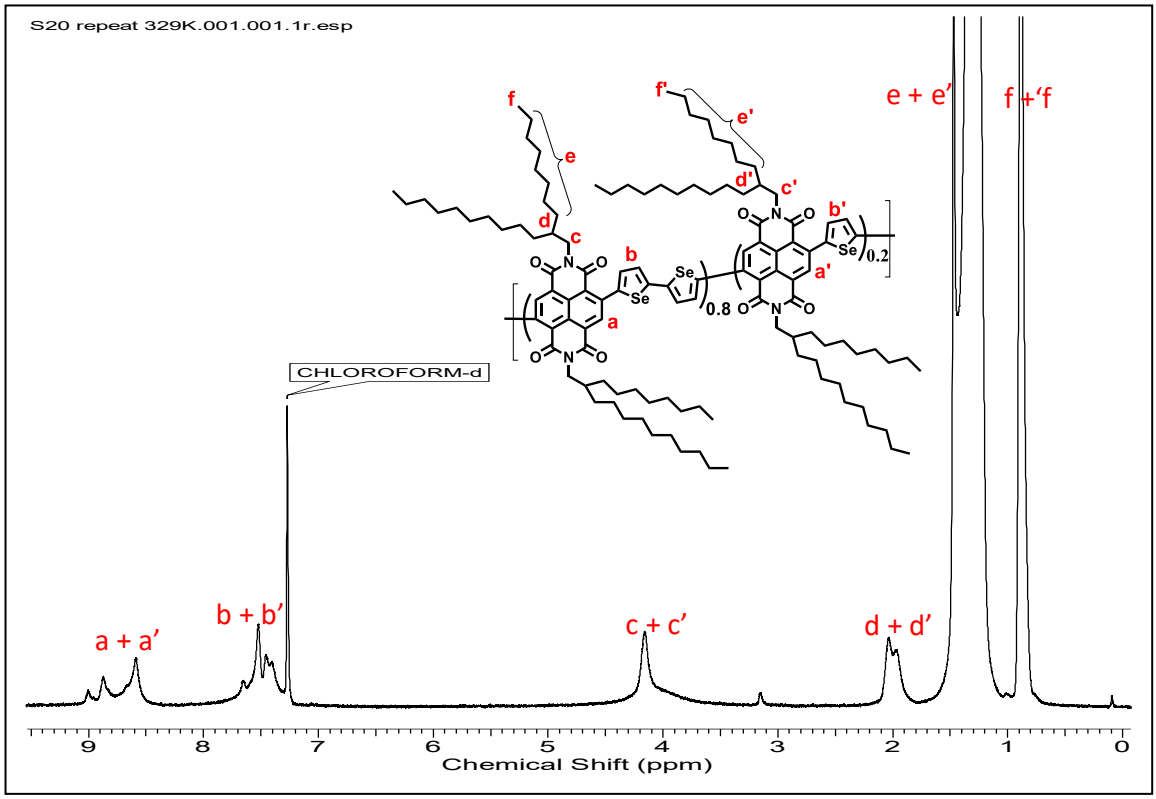

Figure S1b. ^{1}H NMR spectrum of BSS20 in $CDCl_3$ at 329K.

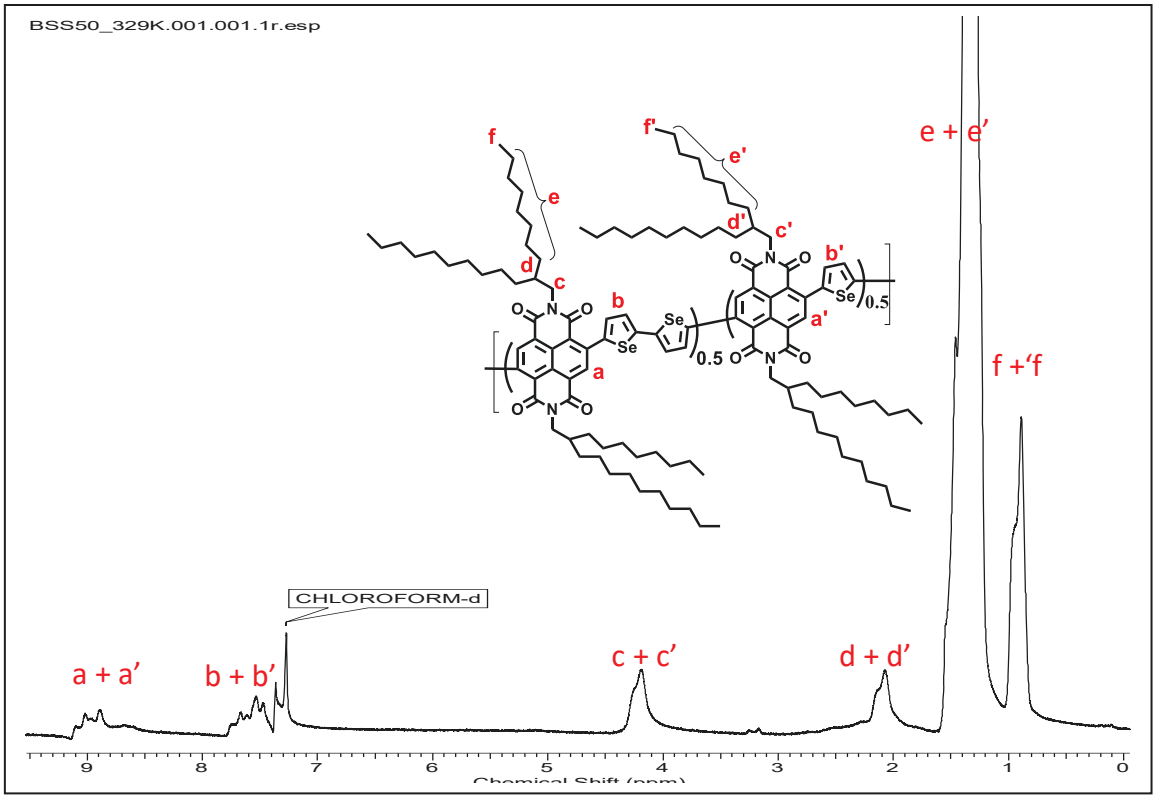

Figure S1c. ^{1}H NMR spectrum of BSS50 in $CDCl_3$ at 329K.

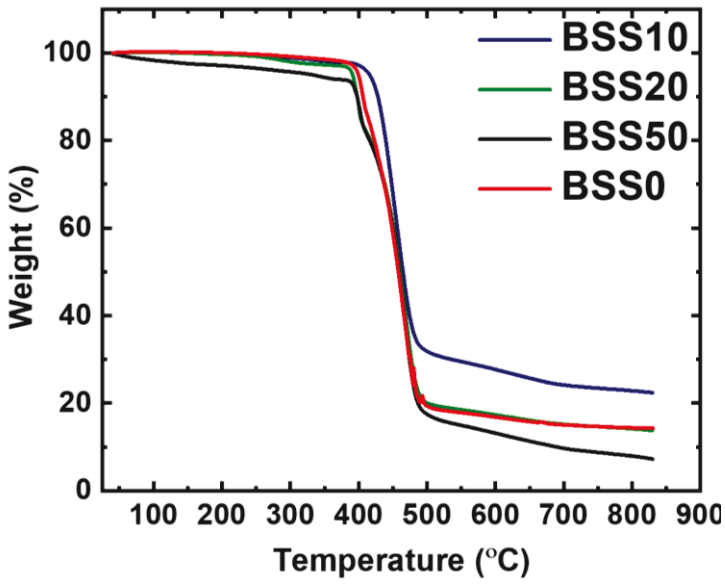

Figure S2. TGA traces of BSS*x* copolymers, at heating rate 10 ºC/min under N_2 gas.

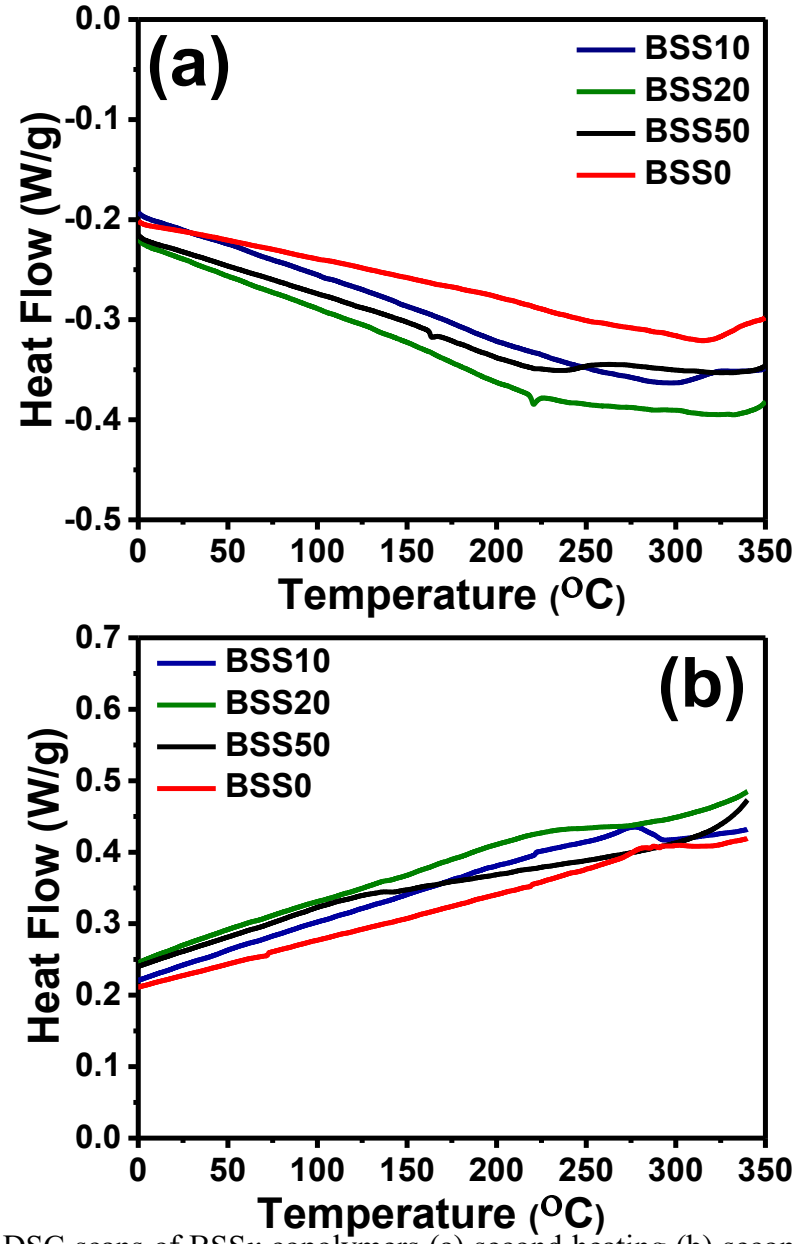

Figure S3. DSC scans of BSS*x* copolymers (a) second heating (b) second cooling, at 10 ºC/min under N_2 gas.

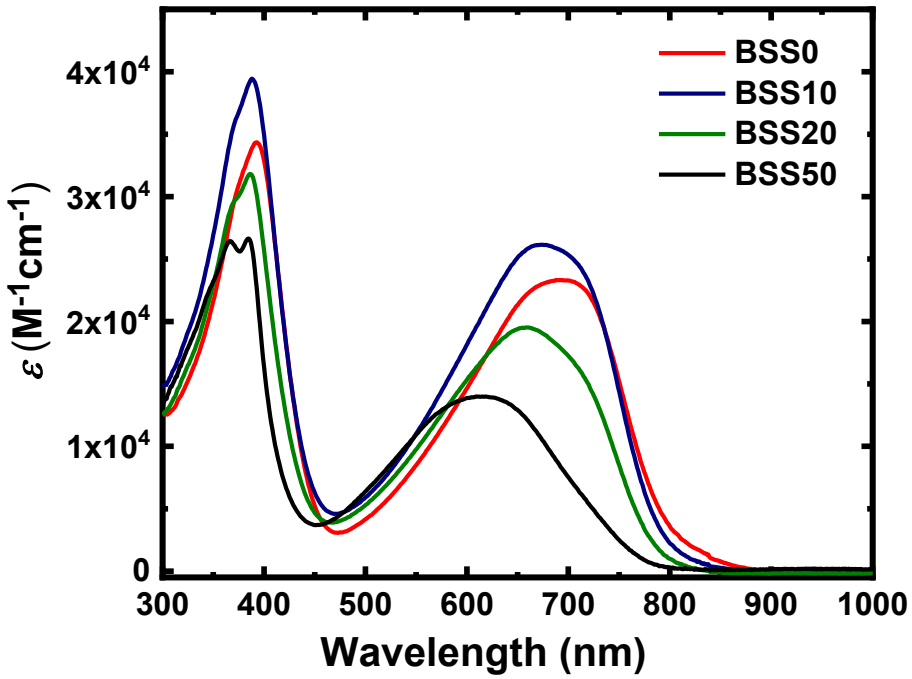

Figure S4. Optical absorption spectra of BSS*x* copolymers in dilute chloroform (1 x 10^{-5} M).

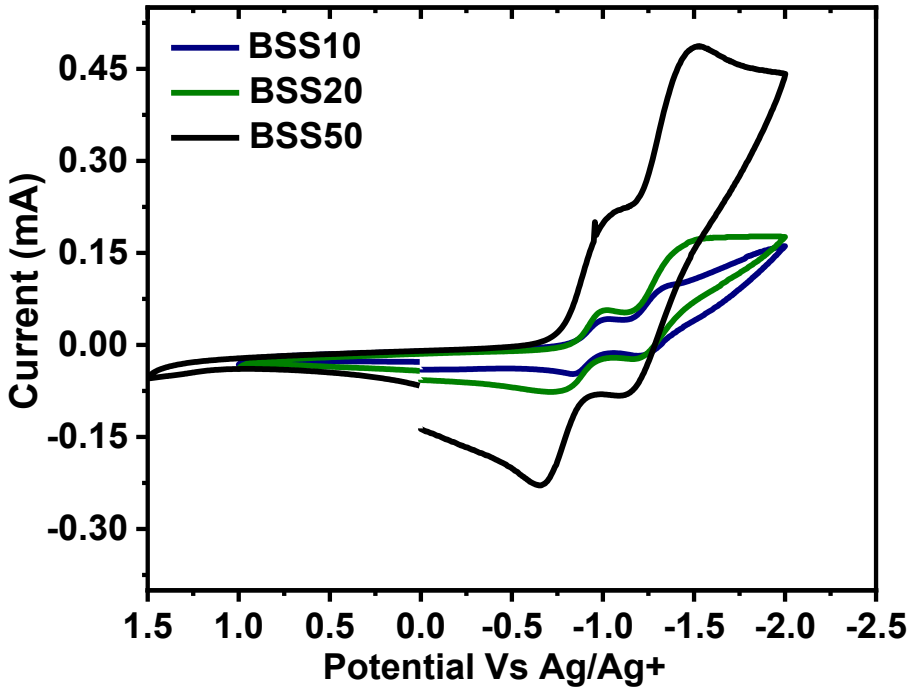

Figure S5. Cyclic voltammograms of BSS*x* thin films in 0.1 M Bu_4NPF_6 solution in acetonitrile at a scan rate of 50 mV s^{-1}.

Table S1. Molecular Weight and Physical Properties of Copolymer Acceptors BSS*x*.

polymer	M_n (kDa)	$Đ$	λ_{max} (nm) [a] ($\log \varepsilon$ $M^{-1}cm^{-1}$)	λ_{max} (nm)[b]	E_g^{opt} (eV)	T_d (℃)	ΔH_m (J/g)
BSS0	28.4	2.88	392, 695 (4.36)	393, 720	1.40	396	4.20
BSS10	41.7	2.82	388, 675 (4.41)	393, 703	1.44	406	2.31
BSS20	33.2	2.54	386, 659 (4.28)	392, 698	1.44	386	-
BSS50	39.1	2.02	384, 615 (4.14)	387, 668	1.49	388	1.26

[a] Absorption maximum in dilute chloroform solution. [b] Thin-film absorption maximum.

Table S2. Performance of BSS10:PBDB-T (0.6:1, wt/wt) All-PSCs Derived From Different Processing Additives. All Devices Spin-coated from Chlorobenzene Solution and Annealed at 175 °C for 10 min.

BSS10	J_{sc} (mA/cm^2)	V_{oc} (V)	FF	PCE_{max} (%)	PCE_{ave}[(a)] (%)
DIO (0.5 vol%)	16.91 (± 0. 06)	0.85 (± 0. 001)	0.62 (± 0. 01)	9.05	8.90 (± 0. 16)
DPE (0.5 vol%)	17.54 (± 0. 25)	0.86 (± 0. 001)	0.64 (± 0. 01)	9.58	9.32 (± 0. 21)
CN (0.5 vol%)	17.04 (± 0. 34)	0.85 (± 0. 003)	0.63 (± 0. 01)	9.15	9.03 (± 0. 10)
ODT (0.5 vol%)	17.05 (± 0. 60)	0.85 (± 0. 003)	0.62 (± 0. 01)	9.47	9.05 (± 0. 31)

(a) Average PCE values obtained from 4 separate devices.

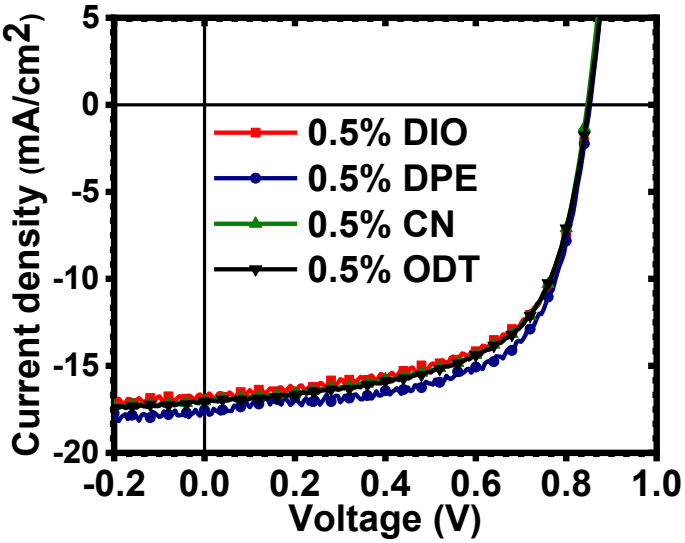

Figure S6. Current density – Voltage (*J-V*) characteristics of BSS10:PBDB-T (0.6:1, wt/wt) all-PSCs derived from different processing additives. All devices annealed at 175 °C for 10 min.

Table S3. Performance of BSS20:PBDB-T (0.6:1, wt/wt) All-PSCs Derived From Different Processing Additives. All Devices Spin-coated from Chlorobenzene Solution and Annealed at 175 °C for 10 min.

BSS20	J_{sc} (mA/cm^2)	V_{oc} (V)	FF	PCE$_{max}$ (%)	PCE$_{ave}$[(a)] (%)
DIO (0.5 vol%)	15.69 (± 0. 64)	0.85 (± 0. 005)	0.65 (± 0. 01)	8.88	8.52 (± 0. 16)
DPE (0.5 vol%)	17.11 (± 0. 47)	0.85 (± 0. 004)	0.64 (± 0. 01)	9.59	9.29 (± 0. 28)
CN (0.5 vol%)	16.02 (± 0. 20)	0.86 (± 0. 01)	0.65 (± 0. 01)	9.02	8.85 (± 0. 12)
ODT (0.5 vol%)	16.96 (± 0. 04)	0.86 (± 0. 001)	0.65 (± 0. 01)	9.62	9.51 (± 0. 09)

(a) Average PCE values obtained from 4 separate devices.

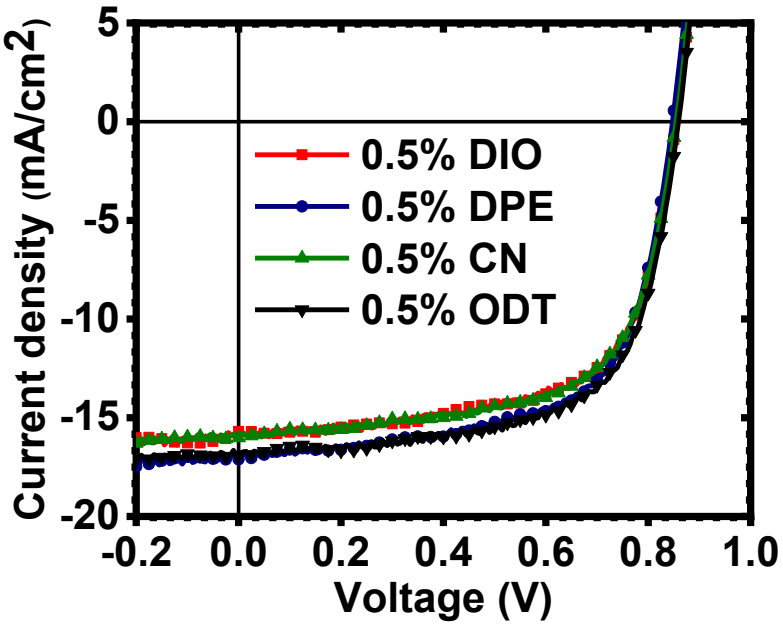

Figure S7. Current density – voltage (*J-V*) characteristics of BSS20:PBDB-T (0.6:1, wt/wt) all-PSCs derived from different processing additives. All devices annealed at 175 °C for 10 min.

Table S4. SCLC Charge Carrier Mobilities of Neat Films of Acceptor Polymers and in the (BSS*x*:PBDB-T) Blend Films Annealed at 175 ºC for 10 min.

Polymer or Blend	μ_e ($cm^2 V^{-1} s^{-1}$)	μ_h ($cm^2 V^{-1} s^{-1}$)	μ_h / μ_e
BSS0	3.49×10^{-5}	-	-
BSS10	1.60×10^{-4}	-	-
BSS20	2.42×10^{-4}	-	-
BSS50	5.35×10^{-5}	-	-
BSS0:PBDB-T	1.69×10^{-5}	1.89×10^{-4}	11.2
BSS10:PBDB-T	6.77×10^{-5}	5.33×10^{-4}	7.88
BSS20:PBDB-T	6.14×10^{-5}	4.43×10^{-4}	7.21
BSS50:PBDB-T	2.18×10^{-5}	6.28×10^{-5}	2.88

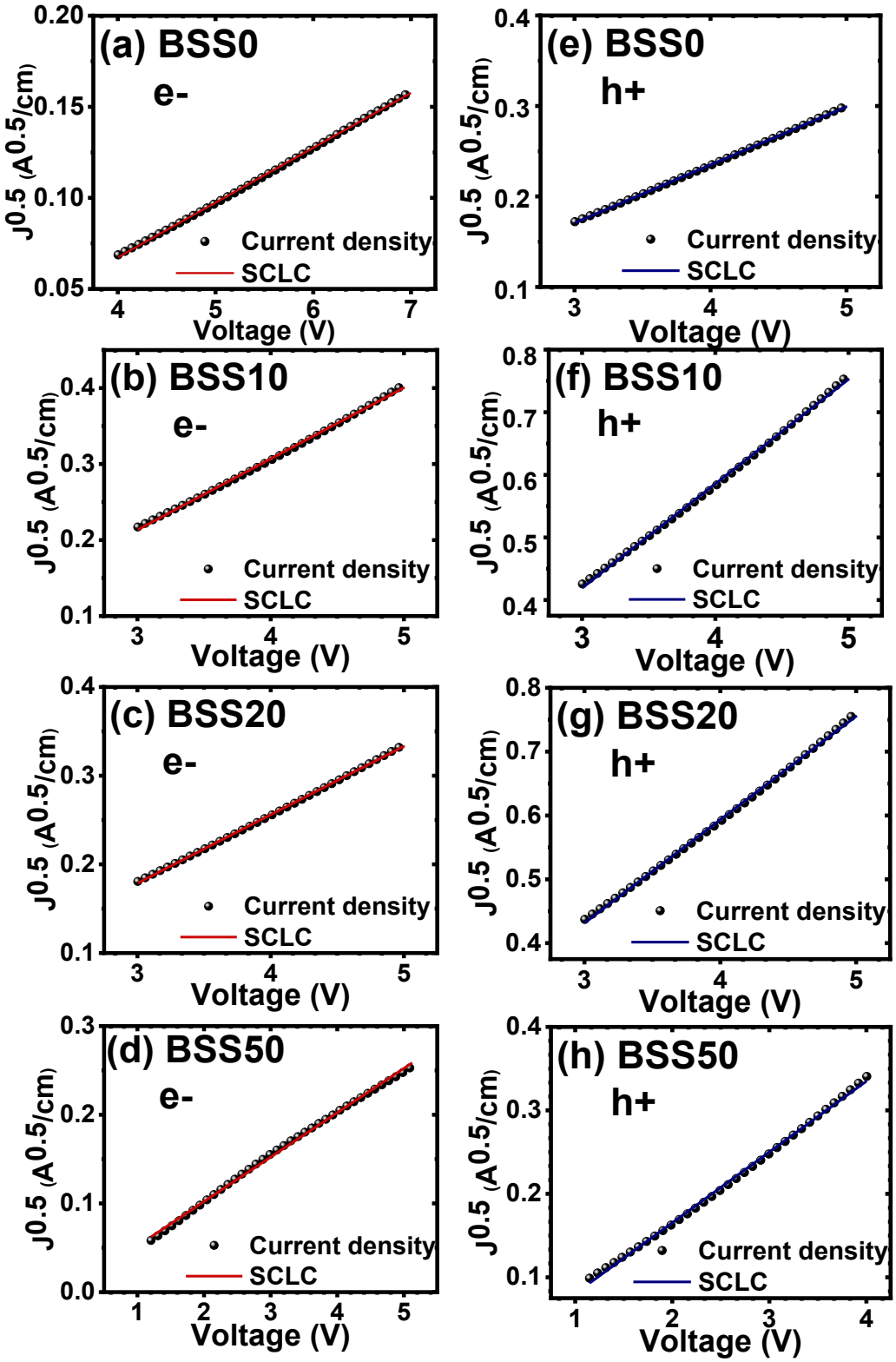

Figure S8. *J-V* characteristics measured by the space-charge-limited current (SCLC) method and fitting for BSS*x*:PBDB-T blends: electron-only devices (a, b, c, d) and hole-only devices (e, f, g, h).

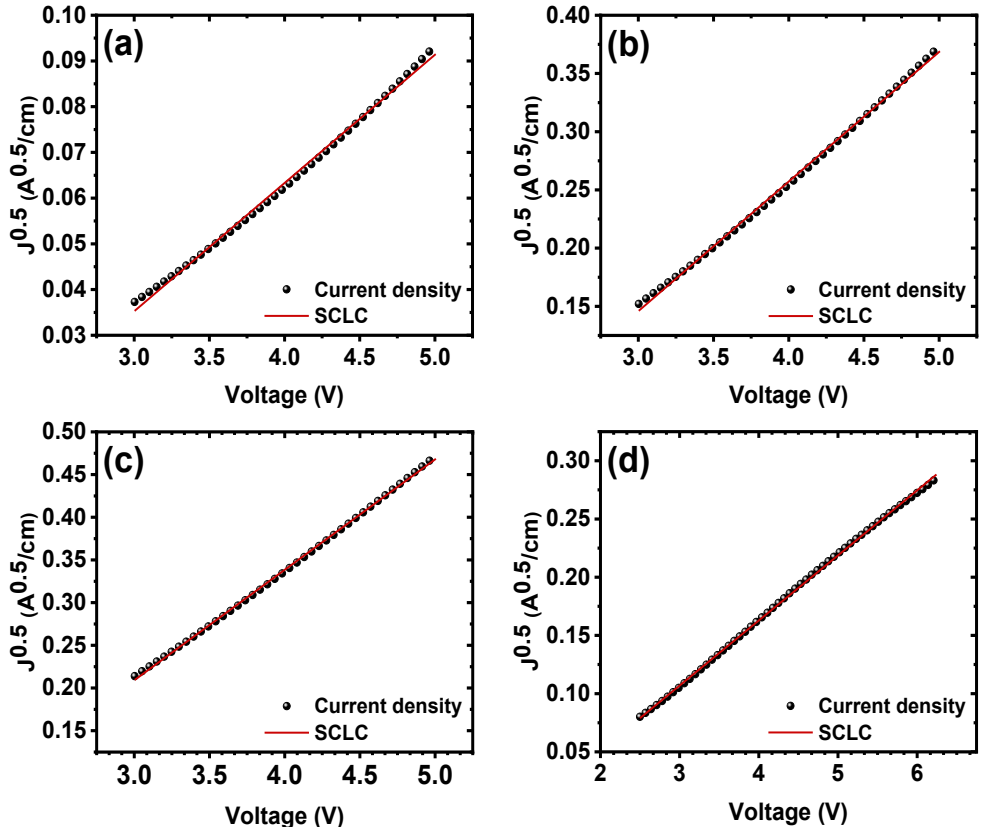

Figure S9. *J-V* characteristics measured by the SCLC method and fitting for BSS*x* neat films (a) BSS0, (b) BSS10, (c) BSS20, and (d) BSS50.

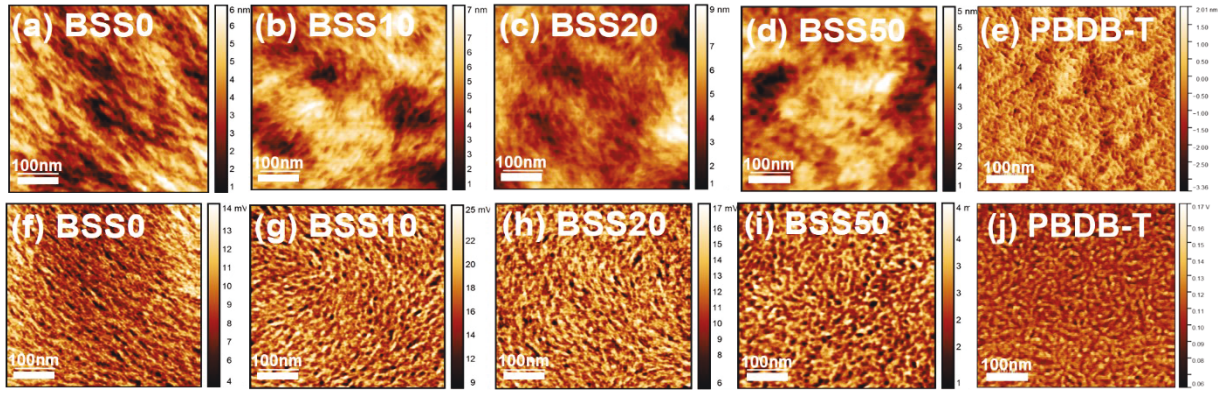

Figure S10. AFM height (a, b, c, d, e) and phase (f, g, h, i, j) images (500 nm x 500 nm) of the surfaces of neat films of BSS*x* acceptor copolymers and PBDB-T donor polymer. The scale bars are 100 nm.

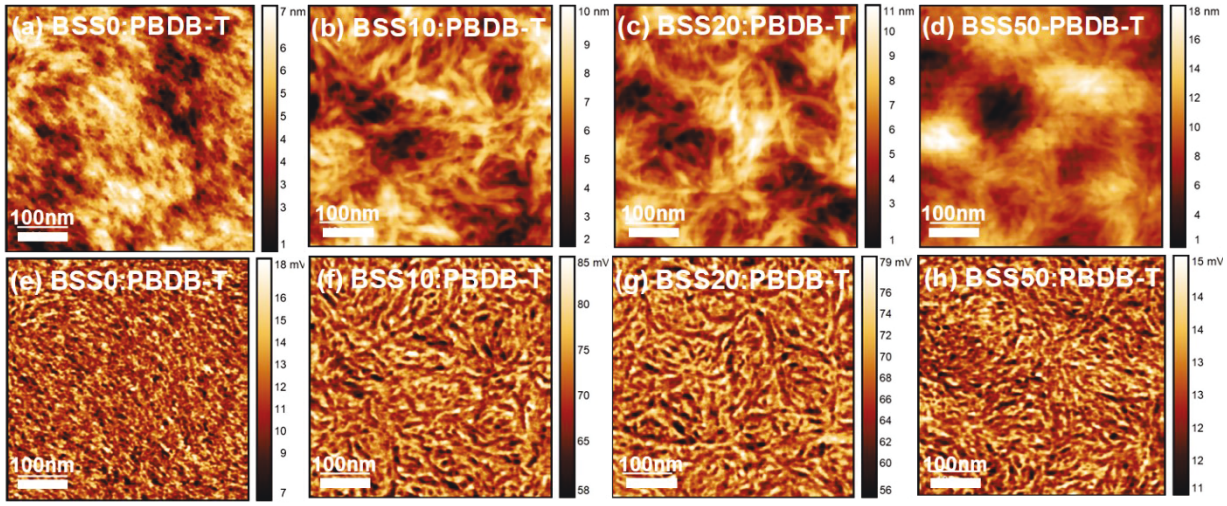

Figure S11. AFM height (a, b, c, d) and phase (e, f, g, h) images (500 nm x 500 nm) of the surfaces of BSS*x*:PBDB-T blend devices. The scale bars are 100 nm.

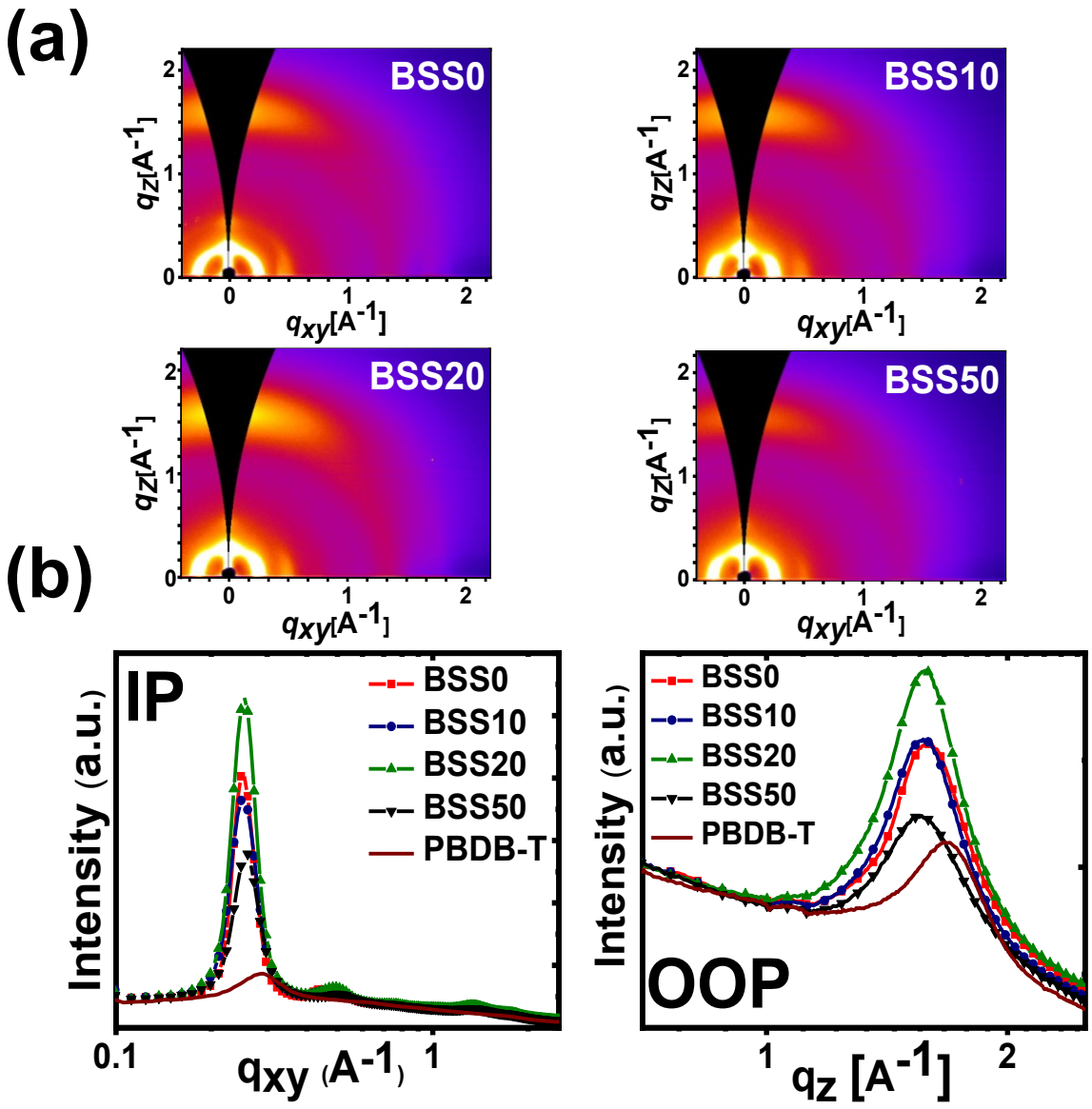

Figure S12. 2D-GIWAXS patterns of neat random copolymer acceptor BSS*x* films (a) In-plane (IP) and out-of-plane (OOP) line cuts of the GIWAXS patterns (b).

Table S5. Crystal Correlation Length (CCL) of Neat Polymer and Blend Thin Films Determined from 2D-GIWAXS.

Sample	(100) [a] Position ($Å^{-1}$)	(010) [b] Position ($Å^{-1}$)	(100) [a] FWHM	(100) [a] CCL nm
Neat PBDB-T	0.28	1.68	1.15	1.3
Neat BSS0	0.25	1.58	0.32	11.6
Neat BSS10	0.25	1.58	0.37	9.7
Neat BSS20	0.25	1.58	0.38	10.7
Neat BSS50	0.25	1.58	0.46	9.7
BSS0: PBDB-T	0.27	1.69	0.84	8.3
BSS10: PBDB-T	0.27	1.69	0.89	7.3
BSS20: PBDB-T	0.27	1.69	0.93	7.3
BSS50: PBDB-T	0.27	1.69	0.83	6.4

[a)] Determined from the in-plane line cut; [b)] Determined from the out-of-plane line cut.

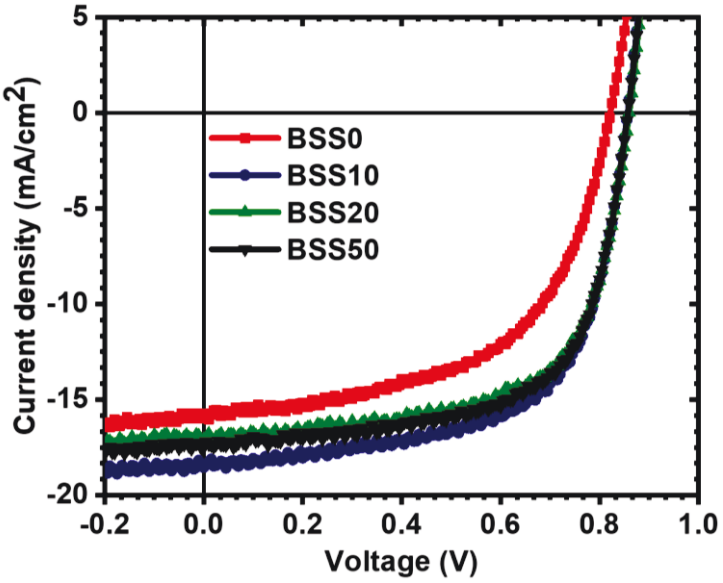

Figure S13. Current density – voltage (*J-V*) characteristics of the highest performing all-PSCs for the optimal BSSx:PBDB-T blends.

References

1. Hwang, Y.-J.; Murari, N. M.; Jenekhe, S. A., New n-type polymer semiconductors based on naphthalene diimide and selenophene derivatives for organic field-effect transistors. *Polym. Chem.* **2013,** *4* (11), 3187-3195.

2. Hwang, Y.-J.; Ren, G.; Murari, N. M.; Jenekhe, S. A., n-Type Naphthalene Diimide–Biselenophene Copolymer for All-Polymer Bulk Heterojunction Solar Cells. *Macromolecules* **2012,** *45* (22), 9056-9062.